

3D FEM approach for laterally loaded monopile design

Murphy, Gerry; Igoe, David; Doherty, Paul; Gavin, K.

DOI

[10.1016/j.compgeo.2018.03.013](https://doi.org/10.1016/j.compgeo.2018.03.013)

Publication date

2018

Document Version

Accepted author manuscript

Published in

Computers and Geotechnics

Citation (APA)

Murphy, G., Igoe, D., Doherty, P., & Gavin, K. (2018). 3D FEM approach for laterally loaded monopile design. *Computers and Geotechnics*, 100, 76-83. <https://doi.org/10.1016/j.compgeo.2018.03.013>

Important note

To cite this publication, please use the final published version (if applicable). Please check the document version above.

Copyright

Other than for strictly personal use, it is not permitted to download, forward or distribute the text or part of it, without the consent of the author(s) and/or copyright holder(s), unless the work is under an open content license such as Creative Commons.

Takedown policy

Please contact us and provide details if you believe this document breaches copyrights. We will remove access to the work immediately and investigate your claim.

3D FEM approach for laterally loaded monopile design

Gerry Murphy¹

David Igoe^{1,2}

P. Doherty¹

K. Gavin^{1,3}

¹Gavin and Doherty Geosolutions, Dublin, Ireland,

²Trinity College Dublin, Ireland

³TU Delft, The Netherlands

Corresponding Author: David Igoe (igoed@tcd.ie)

Over the past 5 years, a substantial research effort aimed at optimising the design of offshore wind turbines has led to significant reductions in the projected cost of developing offshore wind. Optimising the geotechnical design of these structures, through modern analysis techniques such as 3D Finite Element Modelling (FEM), has played a key role in helping to reduce costs. This paper presents a methodology for accurately modelling monopile behaviour using Cone Penetration Test (CPT) data to calibrate the non-linear stress dependent Hardening Soil (HS) model. The methodology is validated by comparing the modelled behaviour to field tests on a range of pile geometries. The paper also demonstrates how the soil-pile reaction response curves can be extracted from the FE model by isolating the stresses on each element of the pile. The contribution of each component to the overall lateral resistance is shown to vary with the pile geometry and is examined using the extracted soil reaction curves.

Keywords:

Offshore foundations; piling; lateral loading; finite element modelling.

1. Introduction

Monopiles are the most commonly used foundation system for supporting offshore wind turbines, accounting for ~80% of all substructures installed to date [1]. Monopile foundations are single large diameter open-ended tubular steel piles, typically driven into the sea bed, which rely on the stiffness and strength of the surrounding soil to provide resistance against large environmental loads from wind and waves. Typical monopile diameters range from 4 – 6m, however due to increasing turbine sizes and applicable water depths, XXL monopiles of up to 10m in diameter are being considered [2]. The slenderness ratio of embedded pile length to diameter (L/D) of a monopile typically varies between 4 and 8, depending on the applied loading and ground conditions, but L/D ratios of 3 or less are anticipated for future XXL monopiles.

1.1 Monopile design practice

The traditional industry standard approach for the geotechnical design of monopiles are those recommended by Det Norske Veritas - Germanischer Lloyd (DNV-GL), which are based on American Petroleum Institute (API) design guidelines, and were originally intended for oil & gas jacket piles. Both guidance documents adopt a Winkler beam approach where the lateral soil reaction at a given depth is described by decoupled non-linear ‘p-y’ curves, where p is the lateral soil reaction and y is the lateral displacement response [3,4]. The methods were calibrated using a limited number of pile tests performed on slender jacket piles with diameters less than 1m, and are generally not valid for large diameter monopiles. Recent editions of the DNV-GL guidelines have been updated to recommend that the p-y curves used for monopile design should be validated by FE analysis, however currently there is no consensus on how this is best achieved in practice.

For the geotechnical design of an individual monopile, a number of limit states must be considered. This paper focuses on the Ultimate Limit State (ULS) and Serviceability Limit State (SLS) pile behaviour as the design pile length is typically governed by these cases. For each individual turbine, a significant number of load cases must be analysed, including time domain analyses for the dynamic response during operation [5]. In addition, the calculated loading is dependent on the structures geometry and the foundation stiffness and therefore requires a number of load-geometry iterations for optimisation. The use of numerical approaches, such as 3D FEM, are now widely adopted in both research and industry for

1
2
3
4
5
6
7
8
9
10
11
12
13
14
15
16
17
18
19
20
21
22
23
24
25
26
27
28
29
30
31
32
33
34
35
36
37
38
39
40
41
42
43
44
45
46
47
48
49
50
51
52
53
54
55
56
57
58
59
60
61
62
63
64
65

modelling complex 3D soil-structure interaction problems. However, when considering the optimisation of an entire offshore wind farm, it becomes clear that relying solely on 3D FEM is too computationally expensive for running all the necessary design iterations and therefore simpler Winkler beam type models are still required [6].

1.2 Current state of the art in monopile geotechnical design

In order to reduce calculation times and improve design efficiency Byrne et al. [2] proposed that the soil reaction curves can be extracted from 3D FE analyses and implemented in a 1D spring model [5]. This method benefits from both the accurate model complexity provided by the 3D FEM and also the reduced computation time of the conventional p-y framework. In order to achieve an accurate representation of the 3D FEM using a 1D Winkler beam model, Byrne et al. [2] extended the traditional ‘p-y’ approach to include additional soil reaction components as follows: (i) the distributed moments, m , due to vertical shaft shear stresses during pile rotation at given depth θ ; (ii) the base shear, S , during horizontal translation at the pile toe and (iii) the base moment, M , during rotation of the pile toe, see Figure 1 [2]. These additional components of soil reaction have been shown to have a significant influence on Monopiles with a slenderness ratio (L/D) of less than 5. The methodology outlined in this paper shows how each soil reaction component can be extracted from a 3D FE Plaxis model, and used as inputs to a 1D FE model to quickly optimise the monopile design and improve design efficiency.

It should be noted that the potential of this approach is entirely dependent on developing 3D FE models which can reliably and accurately capture the monopile response under a range of loading conditions covering small to large strains. To date several studies have been published in which large diameter monopiles have been successfully analysed using commercially available 3D FE packages [7–15], however few have been validated against actual monopile load test results and therefore the accuracy of these models is uncertain.

The calibration of the constitutive soil model to accurately capture the non-linear behaviour over a large strain range is the key challenge when modelling the monopile response. In this paper, the Hardening Soil (HS) soil model was chosen because of its ability to model non-linear soil behaviour, but also for the simplicity of deriving the model input parameters. Several more advanced constitutive soil models, which have the ability to better capture the fundamental critical state mechanics of sands and clays, have been utilised for predicting the

1
2
3
4
5
6
behaviour of laterally loaded piles in recent studies [16–19]. However, there is often an
inherent difficulty in using these models in practice due to difficulties in calibrating the input
parameters which, in some cases, require significant specialised laboratory element testing.

7
8
9
10
11
12
13
14
15
16
17
18
19
20
21
22
23
24
25
26
For most offshore wind farms, only a limited amount of geotechnical information will be
available at an early stage of a project, typically CPT tests and a limited amount of standard
laboratory tests (shear box, triaxial, oedometer, DSS). In addition, the difficulty in acquiring
undisturbed sand samples offshore means that these lab tests are often carried out on
reconstituted samples and may not be representative of the particle interlocking, cementation
and dilatational behaviour of aged dense sand deposits in-situ. Therefore, using a relatively
simple constitutive model which can capture the non-linear soil response (such as the HS
model) and which can be calibrated using in-situ test data such as CPT tests offers a useful
way for designers to estimate the monotonic pile loading response.

27 28 29 30 31 32 **2. 3D FE Modelling**

33 34 35 36 37 38 39 40 41 42 43 44 45 46 47 48 49 50 51 52 53 54 55 56 57 58 59 60 61 62 63 64 65 **2.1 General Modelling Approach**

The monopile field tests described in this paper were modelled using the commercially
available Plaxis 3D 2013 software. The axisymmetric nature of the problem was not
considered and a full mesh was used with the pile positioned at the centre of the mesh. The
finite element mesh used in the analysis is shown in Figure 2. The lateral boundary was set at
forty pile diameters and the depth was set as twice the embedded pile length. The soil
elements were modelled as ten-node tetrahedral elements. The pile wall was modelled as an
18 sided cylindrical plate using six-node plate elements, see Table 1 for number of nodes and
elements in each model. The mesh was generated using the inbuilt Plaxis meshing procedure
and was refined until a satisfactory mesh quality index was achieved. The piles were
modelled as linear elastic elements with Youngs Modulus, $E_p = 200$ GPa, Poisson's ratio, $\nu_p =$
 0.3 and a unit weight of $\gamma = 77\text{kN/m}^3$. Interface elements were also added to the pile shaft.
The reduction in interface shear strength when slip occurs is accounted for using the strength
reduction factor $R_{\text{inter}} = 0.7$ which was in agreement with previous studies at the test site [20].
It should be noted that site specific calibration of all parameters including the shear strength
reduction factor is essential for accurate modelling of the soil-pile system. In order to account
for pile installation affects and the increased stresses in the vicinity of the pile base as a result

of 'locked-in' residual loads developed during pile driving, a vertical jacking phase was applied to the 3D FE model pile prior to application of the lateral loading phases. The use of a jacking phase to model installation effects is described in greater detail in section 4.

2.2 Development of Soil Model

The field tests were modelled using commercially available finite element software Plaxis 3D – 2013. The HS model, as described by Schanz [21], was adopted to define the soil stiffness behaviour. The HS parameters were derived using correlations with the CPT cone resistance (q_c) at both sites. The first step in the design process was the discretisation of the CPT profiles for the upper and lower level test sites, as shown in Figure 3a. The peak friction angle, φ , was estimated accounting for density and stress level effects using Equations 1, 2 & 3 [22–24].

$$\varphi = 17.6 + 11 \log \left[\left(\frac{q_t}{P_a} \right) / \left(\frac{\sigma'_{vo}}{P_a} \right) \right]^{0.5} \quad [\text{Eq. 1}]$$

$$\psi = (\varphi - \varphi'_{cv}) / 0.8 \quad [\text{Eq. 2}]$$

$$D_r^2 = \frac{\frac{q_c}{P_a}}{350 \left(\frac{\sigma'_{vo}}{P_a} \right)^{0.5}} \quad [\text{Eq. 3}]$$

Where: q_t is the cone tip stress corrected for pore water effects, σ'_{vo} is the effective vertical stress ($\sigma'_{vo} = \sigma'_1$) calculated using an effective unit weight of 20 kN/m³, P_a is the reference atmospheric pressure (=100kPa), ψ is the dilation angle, φ'_{cv} is the constant volume friction angle calculated from simple laboratory tests and D_r is the relative density (%). The in-situ soil stress state calculated using Equations 4, 5 & 6 [25,26].

$$OCR = \left[\frac{1.33 * q_t^{0.22}}{K_{0NC} * \sigma'_{vo}^{0.31}} \right]^{\frac{1}{\sin \phi - 0.27}} \quad [\text{Eq. 4}]$$

$$K_{0NC} = 1 - \sin \varphi \quad [\text{Eq. 5}]$$

$$K_0 = K_{0NC} * OCR^{\sin \varphi} \quad [\text{Eq. 6}]$$

Where: OCR is the overconsolidation ratio of the soil, K_{0NC} is the lateral stress coefficient for normally consolidated soils and K_0 describes the effect of OCR on the lateral stress coefficient [27].

The stiffness characteristics of the HS model were defined for each layer based on the empirical correlations for the constrained tangent stiffness modulus E_{oed} from Kulhawy & Mayne (1990), the secant stiffness modulus E_{50} was calculated using Hooke's law as described by Brinkgreve et al. (2012) [27,28].

$$E_{oed,NC} = q_c 10^{1.09 - 0.0075 D_r} \quad [\text{Eq. 7}]$$

$$E_{oed,OC} = q_c 10^{1.78 - 0.0122 D_r} \quad [\text{Eq. 8}]$$

$$E_{50} = \frac{(1-2\nu)(1+\nu)}{1-\nu} E_{oed} \quad [\text{Eq. 9}]$$

$$E_{ur} = 3 \times E_{50} \quad [\text{Eq. 10}]$$

Where: $E_{oed,NC}$ and $E_{oed,OC}$ are the constrained tangent oedometer modulus for normally and over consolidated sands, E_{50} is the secant stiffness modulus calculated following Hooke's law and E_{ur} is the unload-reload stiffness calculated as recommended in the Plaxis materials manual. As the sand at the Blessington site is overconsolidated, Equation 8 was adopted to derive the E_{oed} value. These moduli are dependent on the in-situ stress following the shape of the power function, m , given in Brinkgreve et al. (2012) and are inputted into Plaxis 3D as reference values ($P_a=100\text{kPa}$). The reference moduli are calculated as follows:

$$E_{oed}^{ref} = E_{oed} / \left(\frac{c \cos \varphi - \frac{\sigma'_3}{K_{0NC}} \sin \varphi}{c \cos \varphi + P_a \sin \varphi} \right)^m \quad [\text{Eq. 11}]$$

$$E_{50}^{ref} = E_{50} / \left(\frac{c \cos \varphi - \sigma'_3 \sin \varphi}{c \cos \varphi + P_a \sin \varphi} \right)^m \quad [\text{Eq. 12}]$$

$$E_{ur}^{ref} = E_{ur} / \left(\frac{c \cos \varphi - \sigma'_3 \sin \varphi}{c \cos \varphi + P_a \sin \varphi} \right)^m \quad [\text{Eq. 13}]$$

Where: the exponent m defines the stress dependent stiffness and c is the effective cohesion. Brinkgreve et al. (2012) recommends a value of $m = 0.5$ for sands and silts. The constant

1 parameters used in the hardening soil model for this site are presented in Table 2 and Figure 3
2 presents the cone resistance profile and the interpreted soil stiffness parameters.
3
4
5

6 **2.3 Post Processing Soil Reaction Curves**

7

8
9 Soil reaction curves can be extracted from the 3D FE model for future application into a less
10 computationally intensive 1D spring model. The soil reaction curves can be calculated by
11 examining the stresses acting on the pile structural elements, following the methodologies of
12 [2], [10] and [16]. For each loading stage, the stresses acting on the pile interface elements
13 are outputted at fixed stress points as effective normal stresses and horizontal and vertical
14 shear stresses. The stresses at each gauss point along the pile circumference are resolved into
15 resultant forces acting in the loading (y) direction using Gaussian quadrature. The angle of
16 the each stress relative to the y-direction in the horizontal plane is determined from the
17 coordinates of the node points from the corresponding pile plate elements. The total area of
18 each plate element is determined as the cross product of the corner node coordinates, and the
19 appropriate Gaussian weight factor is applied to each stress point based on the stress point
20 nomenclature, as defined in [28].
21
22
23
24
25
26
27
28
29
30

31
32 The soils distributed reaction force in the y-direction, p , is then calculated at the midpoint of
33 each discretisation depth by summing all the resolved lateral forces acting on the external pile
34 surface over the discretisation interval. Likewise, the distributed moment, m , is calculated
35 from the vertical shear forces acting around the pile centreline. The base shear and base
36 moment are calculated in a similar manner from the stresses acting on the internal pile shaft.
37
38 The profiles of horizontal pile displacement (y) with depth (z) are extracted from the plate
39 elements within Plaxis 3D by generating load-displacement curves at fixed depths
40 corresponding to the mid-point of the elements along the pile for each load stage.
41
42
43
44
45
46
47
48

49 This process is repeated for each discretisation depth and automated using a code
50 implemented in Matlab to reduce calculation time. The forces in the load direction and
51 bending moments along the pile circumference are then used to create bending moment and
52 shear force profiles along the pile shaft. The bending moments along the length of the pile
53 can be calculated from the extracted soil stresses by double integration of the lateral forces
54 (in the y-direction) on the external pile surface, p , and the equivalent forces on the internal
55
56
57
58
59
60
61
62
63
64
65

1 pile surface, s . These are then combined with the distributed moments due to the vertical
2 shear stress acting on the internal and external pile faces as in Equation 14.
3
4

$$5 M_z = F \cdot (h + z) + \iint_0^z (p + s) \cdot dz + \int_0^z (m + m_{int}) \cdot dz \quad [\text{Eqn. 14}]$$

6
7
8
9 where M_z is the bending moment at depth below mudline z , F is the applied load above
10 mudline, h is the height of load application above mudline, m is the distributed moment due
11 to vertical shear forces on the external pile surface and m_{int} is the distributed moment due to
12 vertical shear forces on the internal pile surface. To develop the additional reaction springs
13 proposed by Byrne et al to be implemented in a Winkler beam model, the base shear -
14 displacement, S - y , and base moment-rotation, M_b - θ , can be calculated as:
15
16
17
18
19
20
21

$$22 S = \int_0^L s \cdot dz \quad [\text{Eq. 15}]$$

$$23 M_b = \int_0^L m_{int} \cdot dz \quad [\text{Eq. 16}]$$

24
25
26
27
28
29
30 where L is the pile embedded length. Equilibrium can be checked by comparing the sum of
31 the forces and moments in the load direction to the applied load. A moment equilibrium
32 tolerance of less than 1% was achieved in this study.
33
34
35
36
37
38

39 **3. Field Testing**

40 **3.1 Monopile Static Loading Field Tests**

41
42
43 To validate the FE models, a series of field tests were conducted using prototype scale piles
44 embedded in an over-consolidated dense sand deposit. Four open-ended steel piles with
45 diameters of 245mm and 510mm were driven to embedded lengths between 1500mm and
46 3000mm (with slenderness ration, L/D , between 3 and 6), see Table 1. The piles were
47 installed at two locations in an active quarry. The first (upper) location was excavated more
48 than ten years before the load tests were performed. The second (lower) location was
49 excavated more recently.
50
51
52
53
54
55
56
57
58
59
60
61
62
63
64
65

1 The test site is located in Blessington, approximately 25km south-west of Dublin in Ireland.
2 The site consists of a uniformly graded, horizontally bedded, heavily over-consolidated, and
3 very dense sand deposit. An extensive site investigation comprising CPT, Seismic
4 Dilatometer Testing (SDMT), plate load testing, sonic core sampling, trial pits (for soil
5 classification testing), and in-situ geophysical testing have been undertaken and detailed
6 descriptions of soil properties have been described in previous publications, see [20,29–31].
7 The water table is >10m below ground level (bgl) at the upper site and 2.5m bgl. at the lower
8 site. The CPT q_c profiles shown in Figure 3(a) reveal that the q_c values are notably larger over
9 the top 2m bgl at the lower site. At depths greater than 2m bgl, the profiles become very
10 similar. Test pile P1 was instrumented using strain gauges attached to the tension and
11 compression faces of the pile. The strain gauge data was used to derive bending moment
12 profiles for each load increment applied in a static load test as described in detail by Xue et
13 al. and Murphy et al. [32,33]. The test piles were loaded (using maintained load increments)
14 until pile head displacement continued without the addition of a further load increment. The
15 test configuration used for the 510mm pile was similar to the 245mm tests described in
16 Murphy et al., however, a load eccentricity of 1m was used, compared with an eccentricity of
17 0.4m for the 245mm pile tests. The test load was measured using an in-line load cell, the
18 lateral displacement of the test piles was measured at three locations using linear
19 displacement transducers and the pile rotation was measured using four digital inclinometers.
20 The measured load-displacement response of the field test piles are presented in Figure 4
21 (solid lines).
22
23
24
25
26
27
28
29
30
31
32
33
34
35
36
37
38
39
40

41 **4. Analysis and 3D FE Model Validation**

42
43
44 Once each model run was completed, the load-displacement and soil reaction curves were
45 extracted from each load stage using the displacement and stresses acting along the pile shaft,
46 following the procedure outlined previously. A comparison of the Plaxis model outputs with
47 the field tests is shown in Figure 4 which demonstrates the excellent agreement between the
48 FEM displacements and the measured ground line displacements for all piles.
49
50
51
52
53

54 **4.1 Consideration of Installation Stresses**

55
56
57 The bearing capacity and stiffness response of a pile in sand is primarily dependent on the
58 sand density and the in-situ stress state. Pile installation by driving will result in large shear
59
60
61
62
63
64
65

1 strains and a significant increase in stress along the shaft and near the pile tip. These changes
2 will increase the lateral bearing capacity and are critically dependent on the degree of
3 plugging experienced by the pile during installation, see [31,34]. Most current numerical
4 studies do not take installation effects into account, however some recent studies have
5 examined this issue in detail and with some success using more advanced constitutive soil
6 models [35,36].
7
8
9

10
11
12 Gavin and Lehane (2005) observed that the average base stress mobilised during a hammer
13 blow is in the range of 10 – 20% of the q_c value [37]. When pile driving ceases a residual
14 stress will remain at the pile tip, resulting in ‘locked-in’ stress in the vicinity of the pile base.
15
16 Despite the increase in sophistication and computational power of commercially available
17 FEM software most FEM codes do not permit the full simulation of the pile installation and
18 the piles are simply “wished in place” with only the overburden stresses acting on the pile.
19
20 This is due to large mesh distortion issues when considering large deformations [36,38]. In
21 this paper, a hybrid approach was adopted to approximate the residual base stresses generated
22 during pile driving. Firstly, the pile is “wished in place”, then a series of vertical
23 displacements were applied to the pile head to push (or jack) the pile a small distance into the
24 soil mesh. Small vertical displacement increments ($\approx 1\%D$) were used to approximate the
25 final stages of pile driving. The stresses at the pile base were examined at each displacement
26 stage. Due to the uncertainty over the residual forces locked into field piles after driving, and
27 the difficulties in measuring and separating the internal and external shaft friction of field
28 piles, an approximation of the stress increase caused by pile driving was made. As an initial
29 test, the vertical head displacement was increased in increments until an approximate ten-fold
30 increase in mean effective stress (p') was obtained numerically at the pile base, see Figure 5.
31
32 The models were then reset and the pile was wished in place, the chosen vertical
33 displacement (to achieve the ten-fold increase in p') was then applied prior to the lateral
34 loading being applied. The resulting vertical stress at the base corresponded to approximately
35 15 – 20 times the in-situ vertical stress, σ'_{v0} , or around 2 – 5 % of the CPT cone resistance, q_c ,
36 which was deemed to be an appropriate estimate of the residual base stress for an open-ended
37 pile. The same process was applied to each model pile with consistent results.
38
39
40
41
42
43
44
45
46
47
48
49
50
51
52
53
54
55
56

57 The benefits of applying a jacking stage in capturing the overall pile response is shown for
58 pile P1 in Figure 6. It is evident that applying the jacking stage provides a better match to the
59
60
61
62
63
64
65

1 overall pile response, albeit slightly over-predicting the initial stiffness. In practice, for full
2 scale offshore wind turbine design, there will typically be a sizeable vertical load component
3 due to the self-weight of the wind turbine structure, which should be included in any FE
4 model. For a conservative (i.e. less stiff) design at full scale, it may be appropriate to include
5 the vertical load component only.
6
7
8
9

10 The modelling approach was further validated by comparing the calculated pile shaft bending
11 moments in P1 to those measured using strain gauges as shown in Figure 7 [33]. A
12 comparison of sample p-y curves extracted from the pile P1 “Jacked” and “Wished-in-Place”
13 models are provided in Figure 8. It is evident that applying a jacking stage only has a minor
14 influence on the p-y curves at shallow and mid-depths, but significantly affects the p-y curves
15 in the high stress zone near the pile toe.
16
17
18
19
20
21
22

23 **4.2 Effect of slenderness ratio on soil reaction components**

24 To gain a better understanding of the effect of pile slenderness ratio (L/D) on the relative
25 contribution of the different soil resistance components, the contribution of each component
26 was calculated as a percentage of the applied moment around the point of rotation (equal to
27 the restoring moment exerted by the soil on the pile). The total moment contribution from the
28 p-y and base shear components (i.e. force components) were calculated by multiplying the
29 component force at each depth interval by its distance from the point of rotation (i.e. point of
30 zero lateral displacement, calculated during each load step) and summing the calculated
31 moments together for each component. The contribution due the distributed moment caused
32 by vertical shaft shear forces was calculated by integrating the distributed moment, m , along
33 the length of the pile shaft. The total moments calculated from each of the soil reaction
34 components was then divided by the externally applied moment (= applied lateral force \times
35 vertical distance to point of rotation) to calculate the ‘Moment Contribution Ratio’ (MCR).
36
37
38
39
40
41
42
43
44
45
46
47
48

49 The MCR values provided by each soil reaction component for pile P4 are shown in Figure 9.
50 The comparison shows that ~90% of the restoring moment comes from the distributed lateral
51 load (MCR_{p-y}) acting along the pile shaft and that the MCR_{p-y} is relatively constant with
52 displacement (i.e. from small to large strains). The moment contribution due to the shear
53 force at the pile base (MCR_{S-y}), vertical stresses acting on the pile shaft ($MCR_{m-\theta}$), base
54 moment ($MCR_{Mb-\theta}$) have a combined contribution of approximately 10%.
55
56
57
58
59
60
61
62
63
64
65

1 Further modelling was conducted to examine the influence pile geometries larger than those
2 used in the prototype tests. Additional analyses were performed on pile P5 ($L=3$, $D=0.76$,
3 $L/D=4$) and P6 ($L=3$, $D=1.02$, $L/D=3$). The relative contribution of each soil resistance
4 component was compared for each L/D ratio in Figure 10. Comparing the percentage
5 contribution of each of the resistance components across the normalised displacement range,
6 y/D , shows that as the L/D ratio decreased, the contribution of the lateral soil reaction MCR_{p-y}
7 also reduced (Figure 10a). As the L/D ratio of the piles reduced, the second order resistance
8 components appeared to make a greater contribution to the stiffness response of the
9 foundation (Figure 10b, c & d). This is generally in agreement with recent research
10 [2,5,6,39].
11
12
13
14
15
16
17
18

19 **5. Conclusions**

20 A methodology for predicting the displacement of laterally loaded monopile foundations
21 using a commercially available finite element code is presented. The modelling procedure
22 was validated by comparing the modelled load-displacement behaviour to the results of a
23 series of field tests on prototype scale monopiles. Pile-Soil stresses obtained from the 3D FE
24 model were analysed and used to obtain site-specific soil reaction curves for each pile.
25
26
27
28
29
30
31

32 An initial analysis of the pile resistance components is presented and the following
33 conclusions were drawn:
34
35
36

- 37 • The comparison shows that ~75 - 90% of the restoring moment from the soil acting
38 on the pile comes from the distributed lateral load (MCR_{p-y}) along the pile shaft for
39 the range of pile geometries and applied loads considered.
40
41
- 42 • As the L/D ratio of the piles reduced, the second order resistance components make a
43 larger contribution to the ultimate moment resistance of the foundation, in agreement
44 with other researchers.
45
46
- 47 • The additional (non p-y) soil reaction components when combined can account for
48 10-25% of the moment resisted by the pile depending on the L/D ratio. Ignoring these
49 effects may result in an overly conservative pile design for low slenderness monopiles
50 ($L/D < 6$) which is in agreement with other researchers.
51
52
53
54
55
56

57 The advantage of the proposed methodology is that the modelling procedure can be
58 completed relatively quickly using design inputs that are available in the majority of
59
60
61
62
63
64
65

1 commercial offshore wind projects. This is particularly useful where it is difficult to obtain
2 reliable undisturbed samples from offshore sites.
3

4 **6. Acknowledgements**

5
6
7 The authors would like to acknowledge the support of the Irish Research Council
8 Employment-Based Postgraduate Programme, Roadstone Ltd. Blessington for access to the
9 test sites and plant and Darren Ward at In-situ SI for conducting the CPT. We would also like
10 to acknowledge the support of the EU funded project LEANWIND.
11
12
13
14
15

16 **7. References**

- 17
18
19 [1] Ewea. The European offshore wind industry. Key Trends Stat 2016 2017:33.
20
21 [2] Byrne BW, Mcadam R, Burd HJ, Houlsby GT, Martin CM, Zdravkovi L, et al. New
22 design methods for large diameter piles under lateral loading for offshore wind
23 applications. Front Offshore Geotech III 2015:705–10.
24
25 [3] API. API Recommended Practice 2A-WSD Planning, Designing, and Constructing
26 Fixed Offshore Platforms—Working Stress Design. 22nd Editi. 2014.
27
28 [4] DNV GL AS. DNVGL-ST-0126 : Support structures for wind turbines. 2016.
29
30 [5] Byrne B, McAdam R, Burd H, Houlsby G, Martin C, Beuckelaers W, et al. PISA: New
31 Design Methods for Offshore Wind Turbine Monopiles. Proceeding Offshore Site
32 Investig. Geotech. Conf., London, UK: 2017.
33
34 [6] Burd H, Byrne B, McAdam R, Houlsby G, Martin C, Beuckelaers W, et al. Design
35 Aspects for Monopile Foundations. Proceeding 19th ICSMGE, Seoul: 2017.
36
37 [7] Fan C, Long J. Assessment of existing methods for predicting soil response of laterally
38 loaded piles in sand. Comput Geotech 2005;32:274–89.
39 doi:10.1016/j.compgeo.2005.02.004.
40
41 [8] Lesny K, Paikowsky S, Gurbuz A. Scale effects in lateral load response of large
42 diameter monopiles. Proc Sess Geo-Denver 2007 Contemp Issues Deep Found 2007.
43
44 [9] Achmus M, Kuo Y-S, Abdel-Rahman K. Behavior of monopile foundations under
45 cyclic lateral load. Comput Geotech 2009;36:725–35.
46 doi:10.1016/j.compgeo.2008.12.003.
47
48 [10] Bekken L. Lateral behaviour of large diameter offshore monopile foundations for wind
49 turbines. Delft University of Technology, 2009.
50
51 [11] Kim Y, Jeong S. Analysis of soil resistance on laterally loaded piles based on 3D soil–
52
53
54
55
56
57
58
59
60
61
62
63
64
65

- 1 pile interaction. *Comput Geotech* 2011;38:248–57.
2 doi:10.1016/j.compgeo.2010.12.001.
- 3
4 [12] Zdravković L, Taborda DMG, Potts DM, Jardine RJ, Sideri M, Schroeder FC.
5 Numerical modelling of large diameter piles under lateral loading for offshore wind
6 applications. *Third Int. Symp. Front. Offshore Geotech. (ISFOG 2015)*, Oslo Norway:
7 2015, p. 759–64.
- 8
9
10 [13] Gupta BK, Basu D. Analysis of laterally loaded rigid monopiles and poles in
11 multilayered linearly varying soil. *Comput Geotech* 2016;72:114–25.
12 doi:10.1016/j.compgeo.2015.11.008.
- 13
14
15 [14] Thieken K, Achmus M, Lemke K. A new static p-y approach for piles with arbitrary
16 dimensions in sand. *Geotechnik* 2015;38:267–88. doi:10.1002/gete.201400036.
- 17
18
19 [15] Lesny K, Wiemann J. Finite-Element-Modelling of Large Diameter Monopiles for
20 Offshore Wind Energy Converters. *GeoCongress 2006*, Reston, VA: American Society
21 of Civil Engineers; 2006, p. 1–6. doi:10.1061/40803(187)212.
- 22
23
24 [16] Zdravković L, Taborda DMG, Potts DM, Jardine RJ, Sideri M, Schroeder FC, et al.
25 Numerical modelling of large diameter piles under lateral loading for offshore wind
26 applications. *Front. Offshore Geotech. III*, Oslo Norway: 2015, p. 759–64.
- 27
28
29 [17] Wang D, Bienen B, Nazem M, Tian Y, Zheng J, Pucker T, et al. Large deformation
30 finite element analyses in geotechnical engineering. *Comput Geotech* 2015;65:104–14.
31 doi:10.1016/j.compgeo.2014.12.005.
- 32
33
34 [18] Khoa HD V, Jostad HP. Application of a Cyclic Accumulation Model UDCAM to FE
35 Analyses of Offshore Foundations. *Proc. 4th Congrès Int. Géotechnique - Ouvrages -*
36 *Structures. CIGOS 2017*, 2017, p. 656–67.
- 37
38
39 [19] Jostad HP, Grimstad G, Andersen KH, Sivasithamparam N. A FE procedure for
40 calculation of cyclic behaviour of offshore foundations under partly drained
41 conditions. *Front Offshore Geotech III* 2015:978–1.
- 42
43
44 [20] Doherty P, Kirwan L, Gavin K, Igoe D, Tyrrell S, Ward D, et al. An Overview of the
45 UCD Geotechnical Research Site at Blessington. In: Caprani C, O’Connor A, editors.
46 *Proc. BCRI 2012*, 6-7th Sept. 2012, Dublin, Dublin, Ireland: Bridge and Concrete
47 Research Ireland; 2012, p. 499–504.
- 48
49
50 [21] Schanz T, Vermeer A, Bonnier P. The hardening soil model: formulation and
51 verification. *Beyond 2000 Comput. Geotech. 10 years PLAXIS Int. Proc. Int. Symp.*
52 *beyond 2000 Comput. Geotech. Amsterdam Netherlands* 1820 March 1999, 1999, p.
53 281.
- 54
55
56
57
58
59
60
61
62
63
64
65

- 1
2
3
4
5
6
7
8
9
10
11
12
13
14
15
16
17
18
19
20
21
22
23
24
25
26
27
28
29
30
31
32
33
34
35
36
37
38
39
40
41
42
43
44
45
46
47
48
49
50
51
52
53
54
55
56
57
58
59
60
61
62
63
64
65
- [22] Bolton MD. The strength and dilatancy of Sands. *Géotechnique* 1986;36:65–78.
 - [23] Kulhawy F, Mayne PW. Manual on estimating soil properties for foundation design. 1990.
 - [24] Lunne T, Christoffersen HP. Interpretation of Cone Penetrometer Data for Offshore Sands. 15th Annu. OTC Houston, TX, May 2-5., 1983.
 - [25] Mayne PW, Kulhawy F. Ko - OCR relationships in soils. *J Geotech Eng Div* 1982;108:851–72.
 - [26] Mayne PW. Stress strain strength flow parameters from enhanced in-situ tests. Proceedings, Int. Conf. In-Situ Meas. Soil Prop. Case Hist. [In-Situ 2001], Bali, Indones., 2001, p. 27–48.
 - [27] Kulhawy F, Mayne PW. Manual on Estimating Soil Properties for Foundation Design. 1990.
 - [28] Brinkgreve RBJ. PLAXIS 3D Reference Manual 2013.
 - [29] Gavin K, O’Kelly B, Adekunle A. A field investigation of vertical footing response on sand. *Proc. ICE - Geotech. Eng.*, vol. 162, 2009, p. 257–67. doi:10.1680/geng.2009.162.5.257.
 - [30] Tolooiyan A, Gavin K. Modelling the Cone Penetration Test in sand using Cavity Expansion and Arbitrary Lagrangian Eulerian Finite Element Methods. *Comput Geotech* 2011;38:482–90. doi:10.1016/j.compgeo.2011.02.012.
 - [31] Igoe D, Gavin K, O’Kelly BC. Shaft Capacity of Open-Ended Piles in Sand. *J Geotech Geoenvironmental Eng* 2011;137:903–13. doi:10.1061/(ASCE)GT.1943-5606.0000511.
 - [32] Xue J, Murphy G, Doherty P, Igoe D, Gavin K. Optimization Technique to Determine the p-y Curves of Laterally Loaded Stiff Piles in Dense Sand. *Geotech Test J* 2016;39:20140257. doi:10.1520/GTJ20140257.
 - [33] Murphy G, Doherty P, Cadogan D, Gavin K. Field experiments on instrumented Winged-Monopiles. *ICE Proc - Geotech Eng Press* 2016;169:227–39. doi:10.1680/jgeen.15.00134.
 - [34] Gavin KG. Behaviour of open and closed ended piles in sand - PhD Thesis. Trinity College Dublin., 1998.
 - [35] Phuong NT V, van Tol AF, Elkadi ASK, Rohe A. Numerical investigation of pile installation effects in sand using material point method. *Comput Geotech* 2016;73:58–71. doi:10.1016/j.compgeo.2015.11.012.
 - [36] Dijkstra J, Broere W, Heeres OM. Numerical simulation of pile installation. *Comput*

Geotech 2011;38:612–22. doi:10.1016/j.compgeo.2011.04.004.

- 1
2 [37] Gavin K, Lehane BM. Estimating the end bearing resistance of pipe piles in sand using
3 the final filling ratio. *Front. Offshore Geotech.*, Perth: Taylor and Francis; 2005, p.
4 717–24. doi:10.1201/NOE0415390637.ch81.
5
6 [38] Dijkstra J, Broere W, van Tol AF. Eulerian Simulation of the Installation Process of a
7 Displacement Pile. *Contemp. Top. Situ Testing, Anal. Reliab. Found.*, Reston, VA:
8 American Society of Civil Engineers; 2009, p. 135–42. doi:10.1061/41022(336)18.
9
10 [39] Lam IP. Diameter Effects on p-y Curves. *Deep Mar Found - A Perspect Des Constr*
11 *Deep Mar Found* 2009;88.
12
13
14
15
16
17
18
19
20
21
22
23
24
25
26
27
28

29 **Table 1: Monopile Test Pile Dimensions**

30 **Table 2: Constant Soil Model Inputs**

31
32
33
34 **Figure 1: Soil reaction curves after [2]**

35 **Figure 2: Typical mesh used in pile analysis**

36 **Figure 3: (a) CPT Profile (b) Peaks Shear Friction Angle (c) & (d) Reference Tangent and**
37 **Secant Stiffness at 100kPa**

38
39 **Figure 4: Load-displacement response of test piles compared to model results**

40
41 **Figure 5: Mean effective stresses p' (a) prior to jacking stage (b) after jacking stage for pile P1**

42 **Figure 6: Comparison of field tests results and modelled pile behaviour for pile P1**

43 **Figure 7: Comparison of the Bending Moment and calculated displacement profiles for pile P1**

44 **Figure 8: Comparison of “Jacked” and “Wished-in-Place” FE models for pile P1 p-y response**

45 **Figure 9: Contribution of each resistance component for pile P2**

46
47 **Figure 10: Contribution of each resistance component for each pile**
48
49
50
51
52
53
54
55
56
57
58
59
60
61
62
63
64
65

Figure
[Click here to download high resolution image](#)

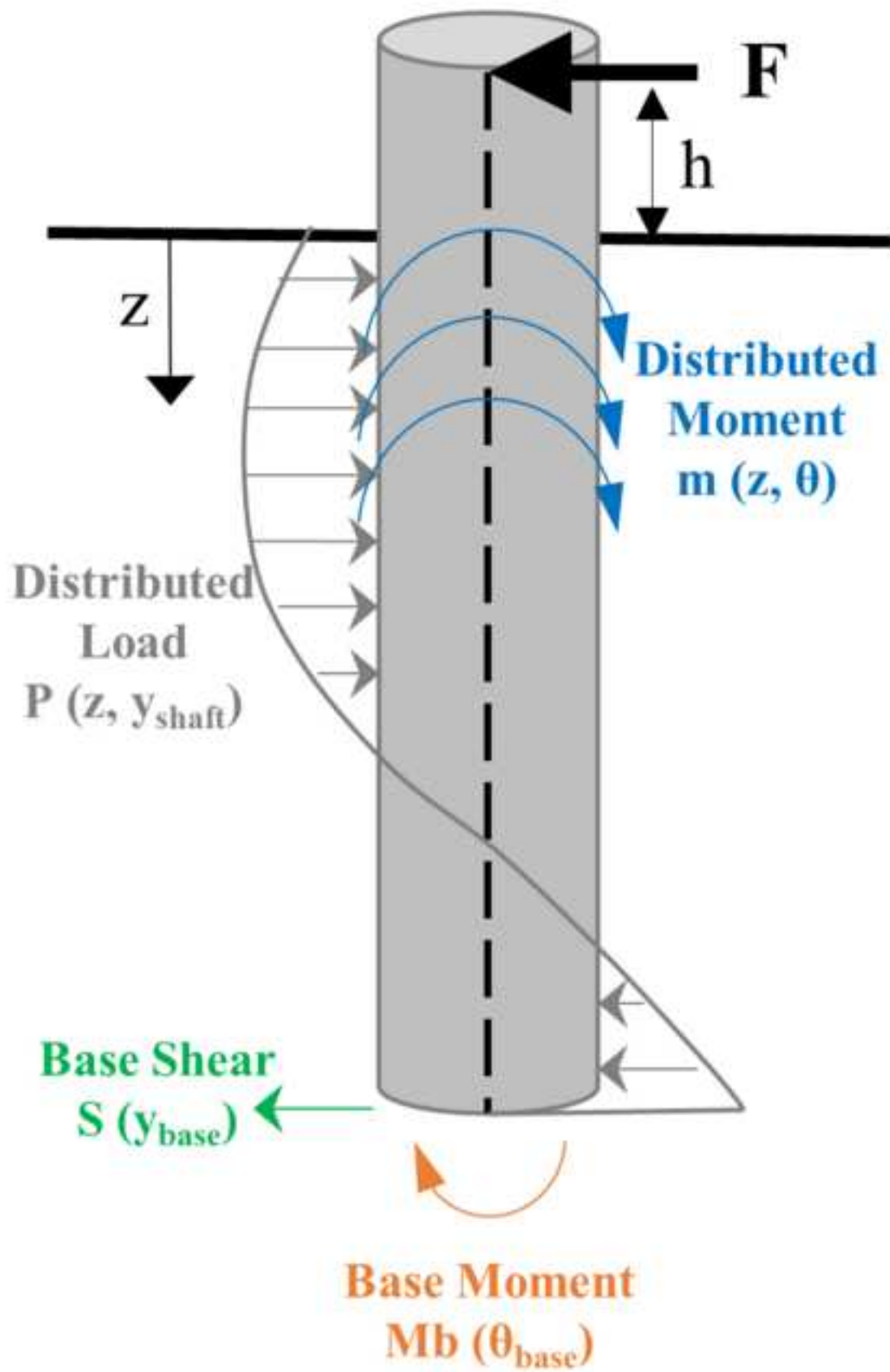


Figure
[Click here to download high resolution image](#)

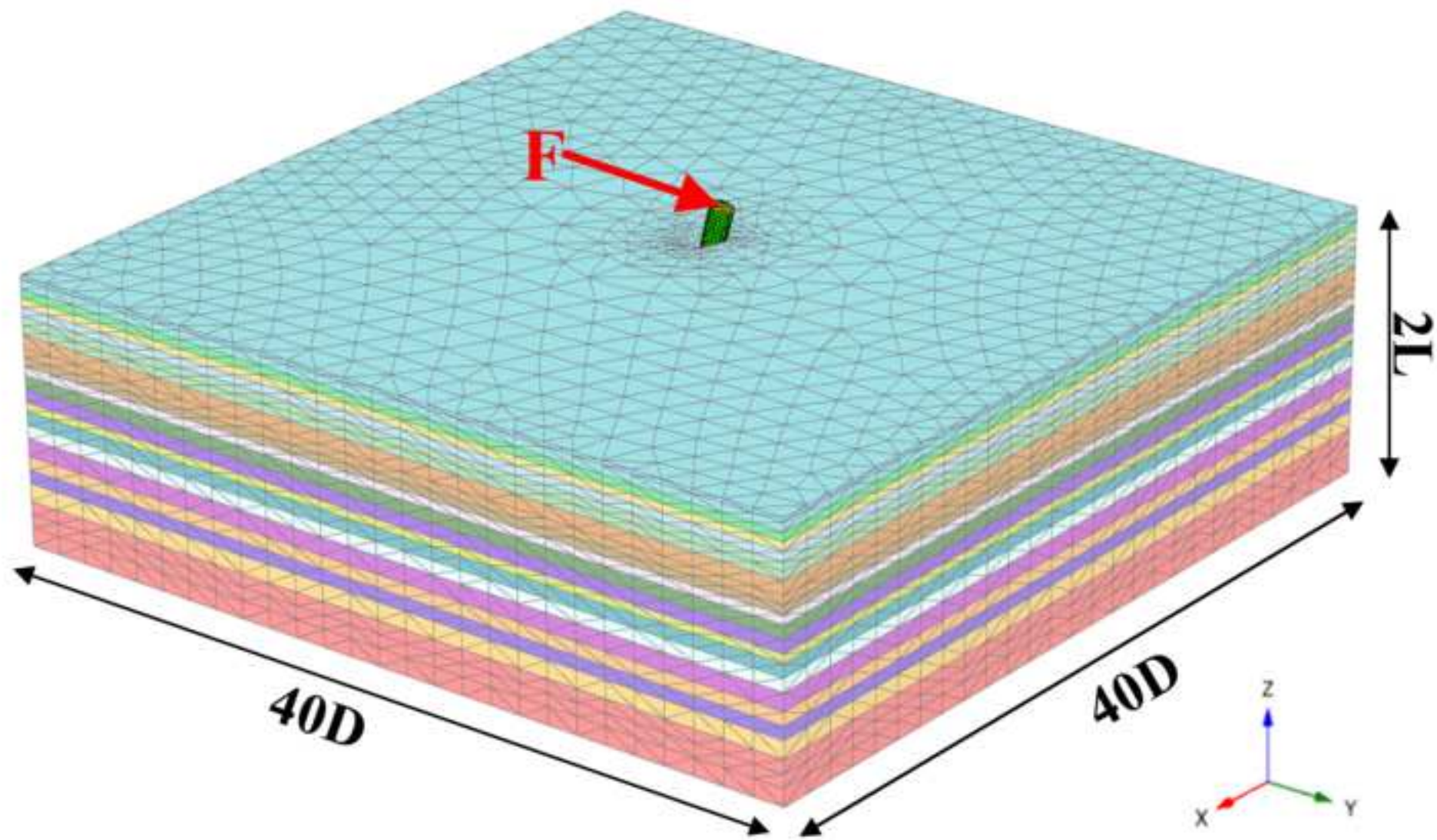


Figure
[Click here to download high resolution image](#)

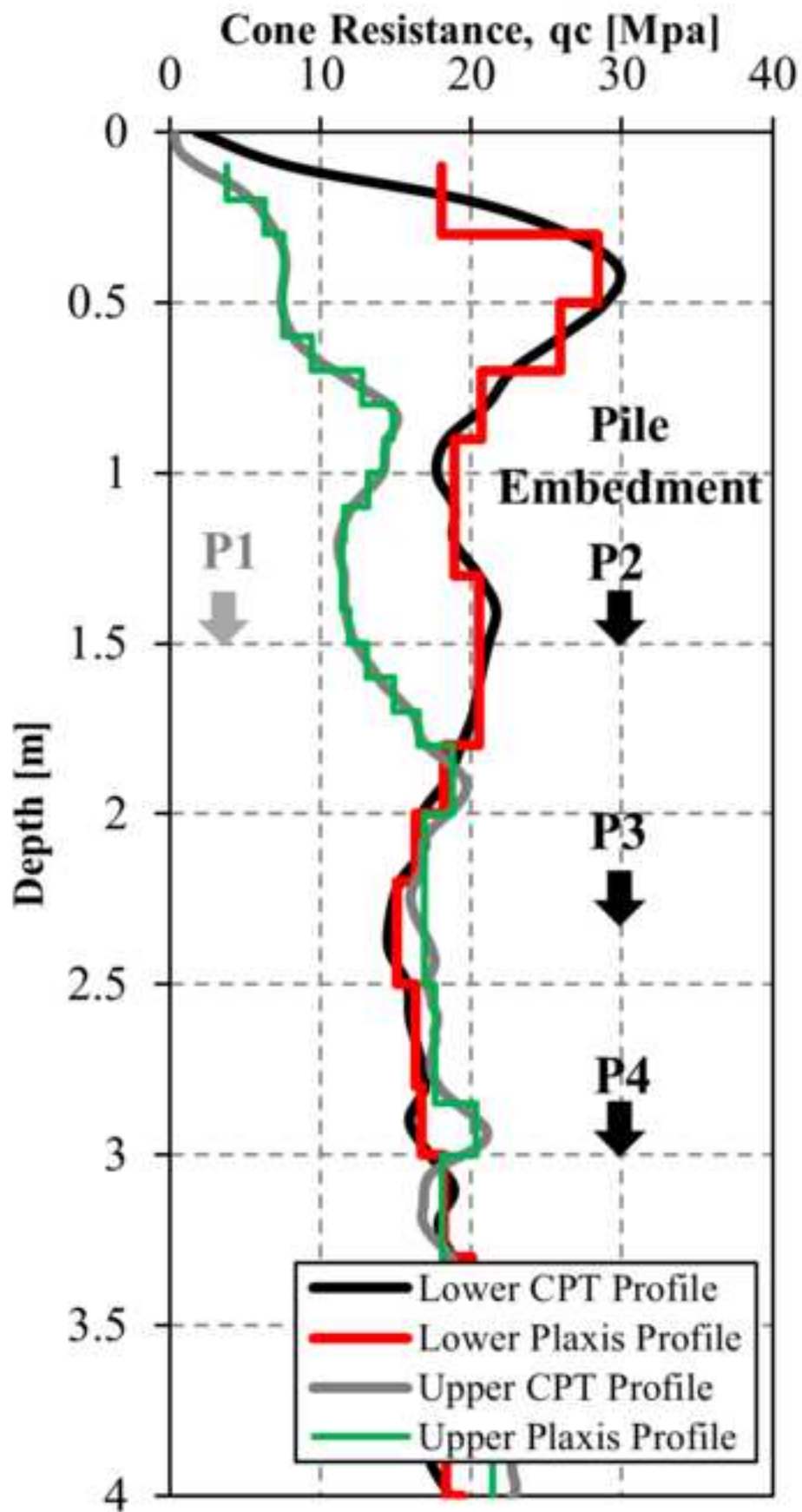


Figure
[Click here to download high resolution image](#)

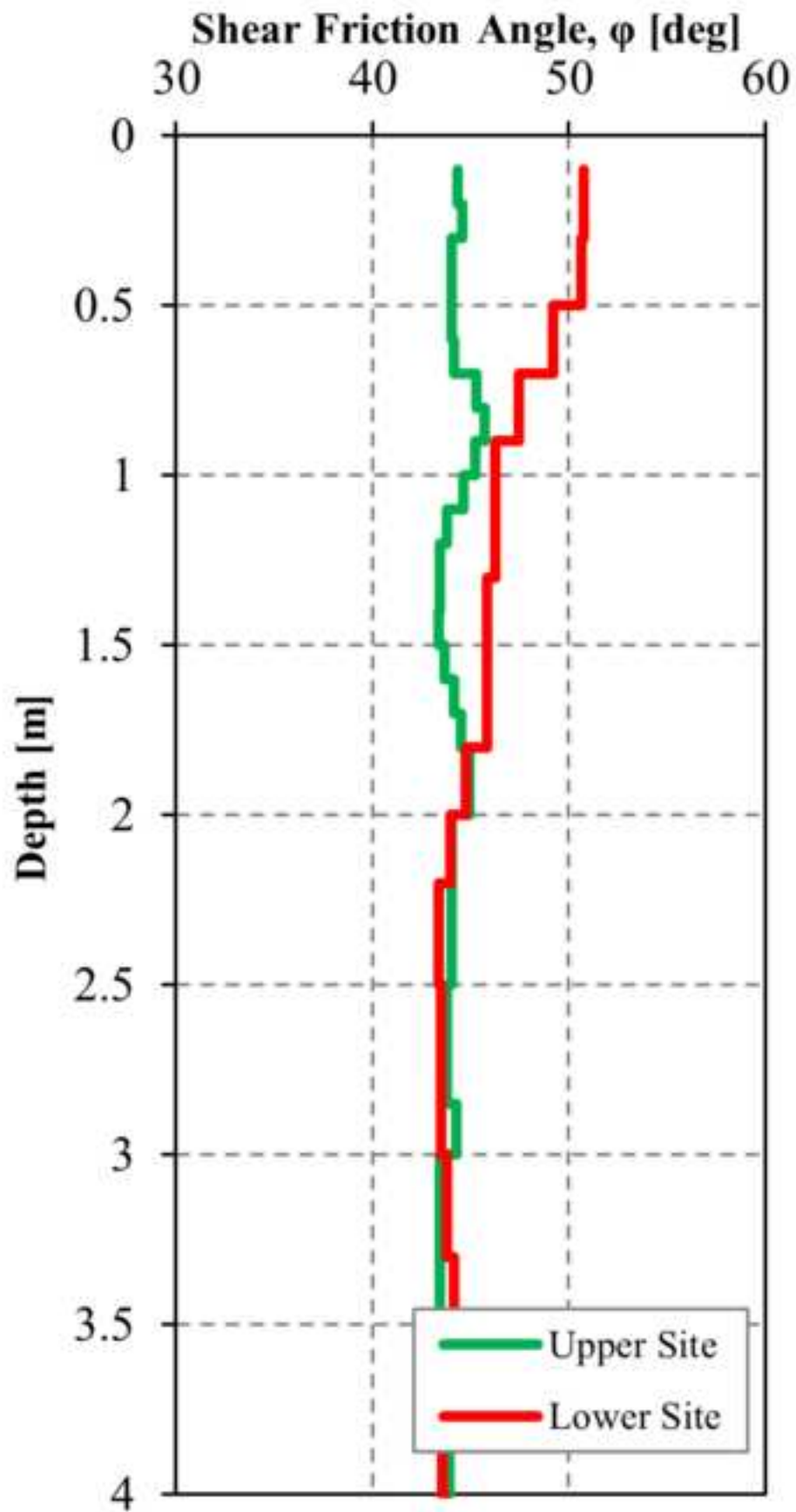


Figure
[Click here to download high resolution image](#)

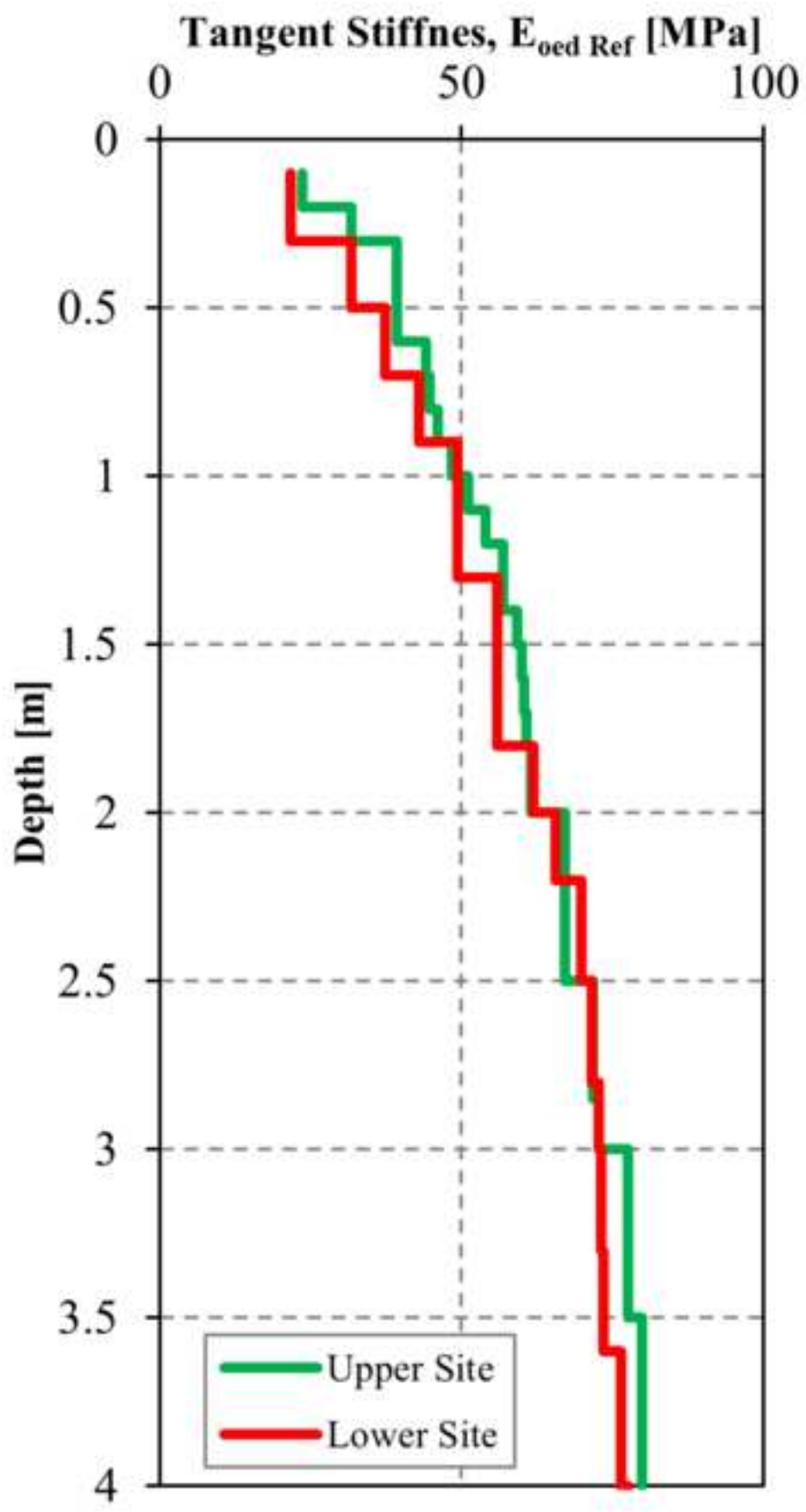
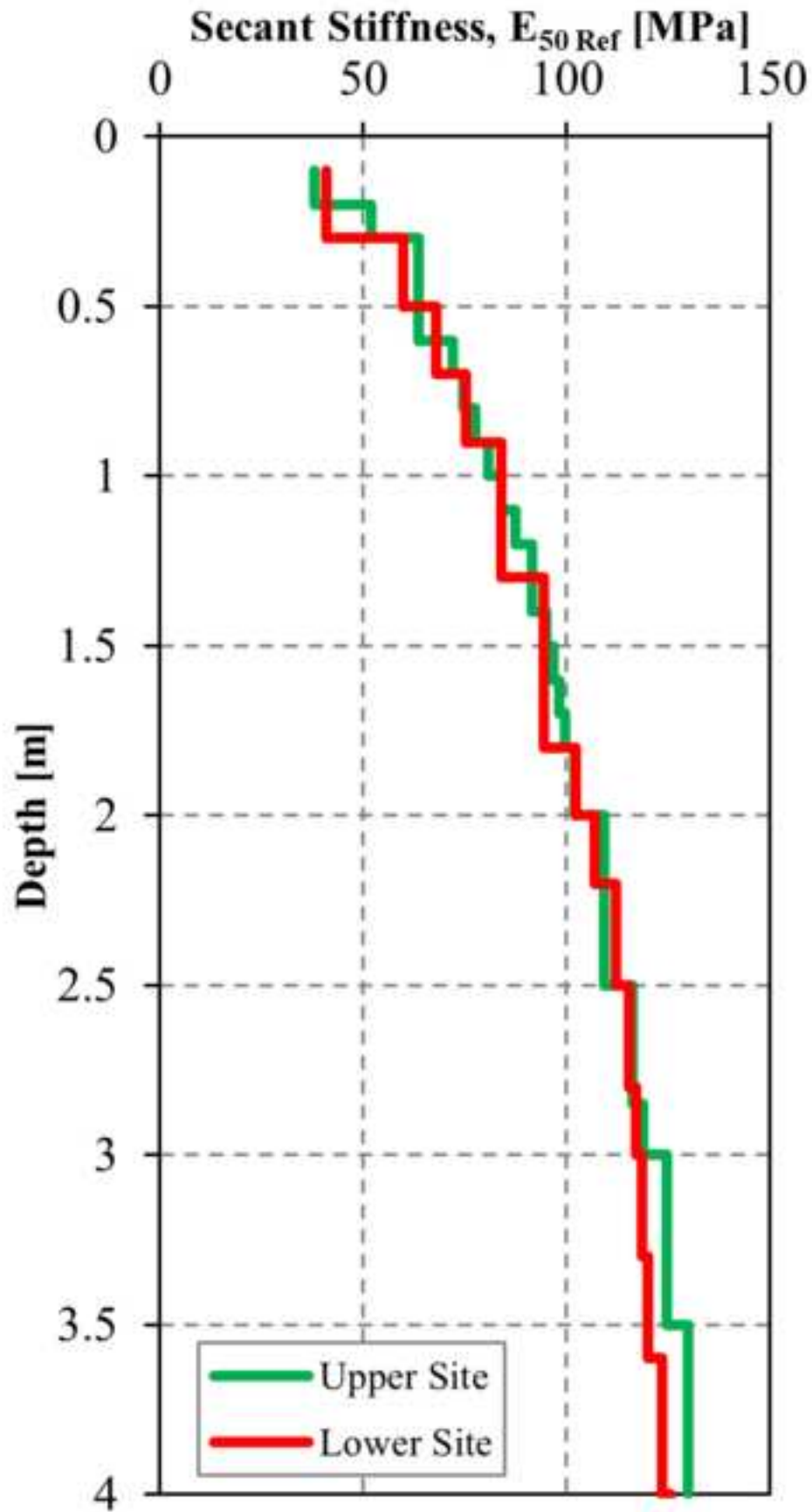


Figure
[Click here to download high resolution image](#)



Figure

[Click here to download high resolution image](#)

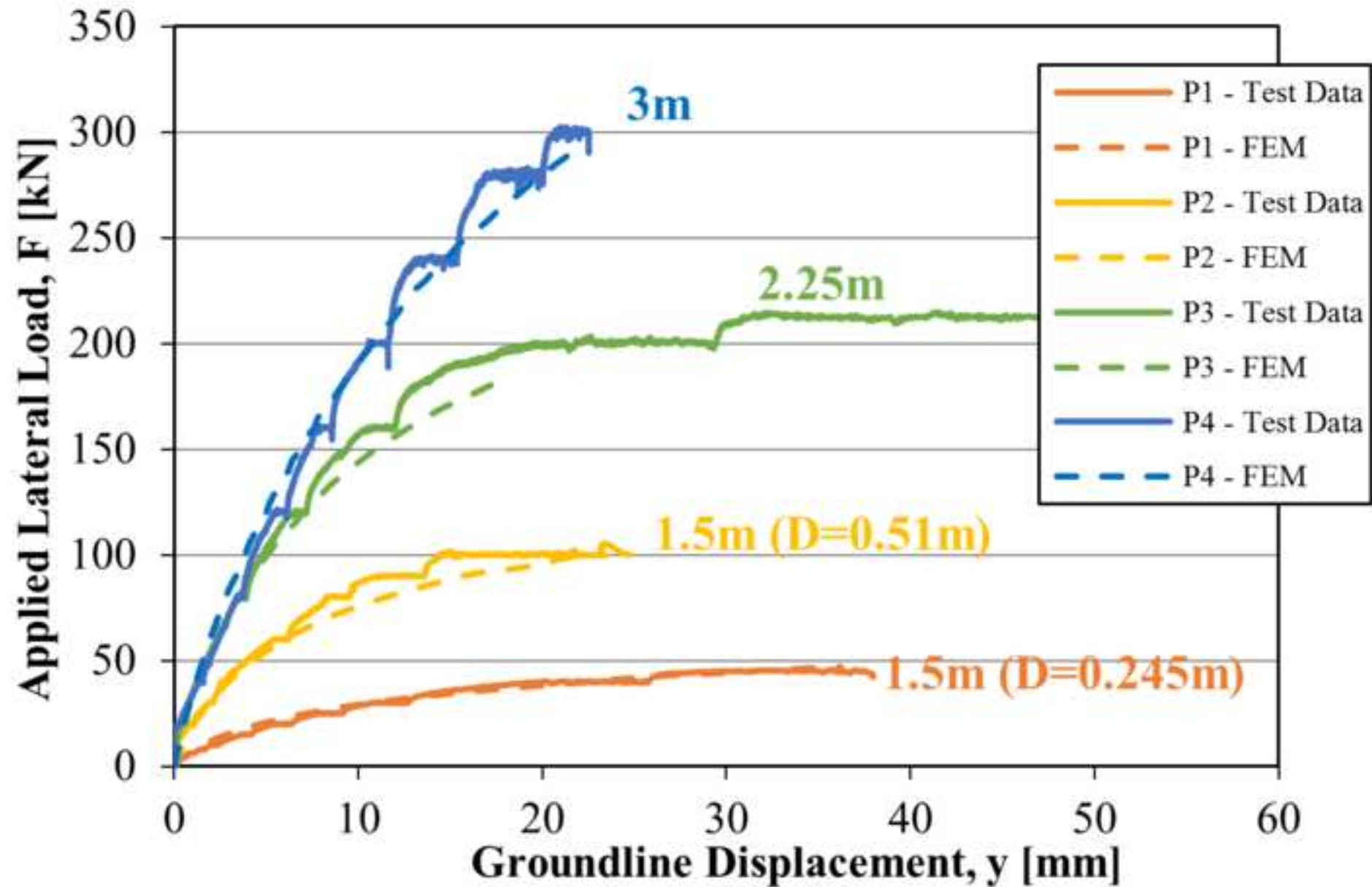


Figure
[Click here to download high resolution image](#)

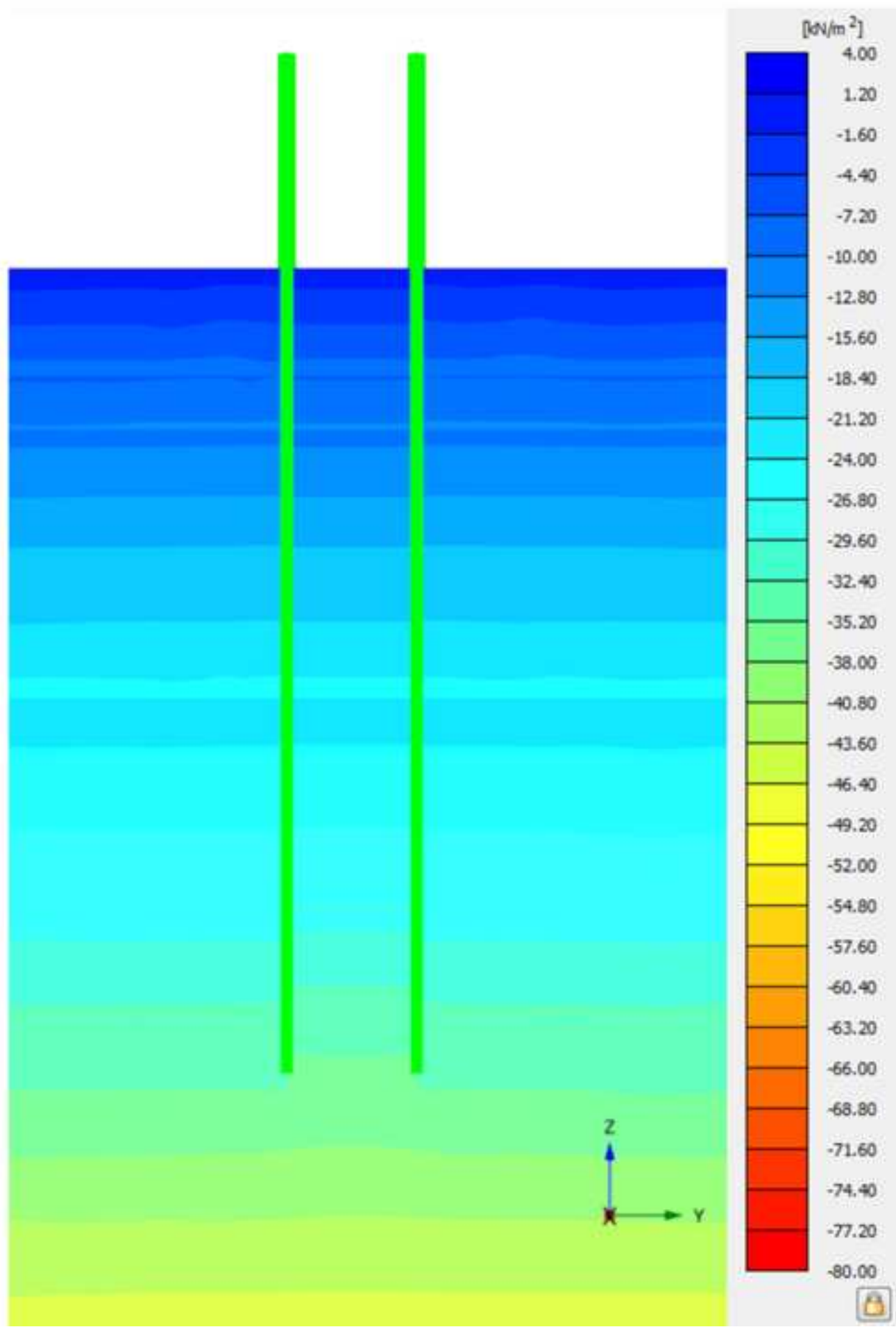


Figure
[Click here to download high resolution image](#)

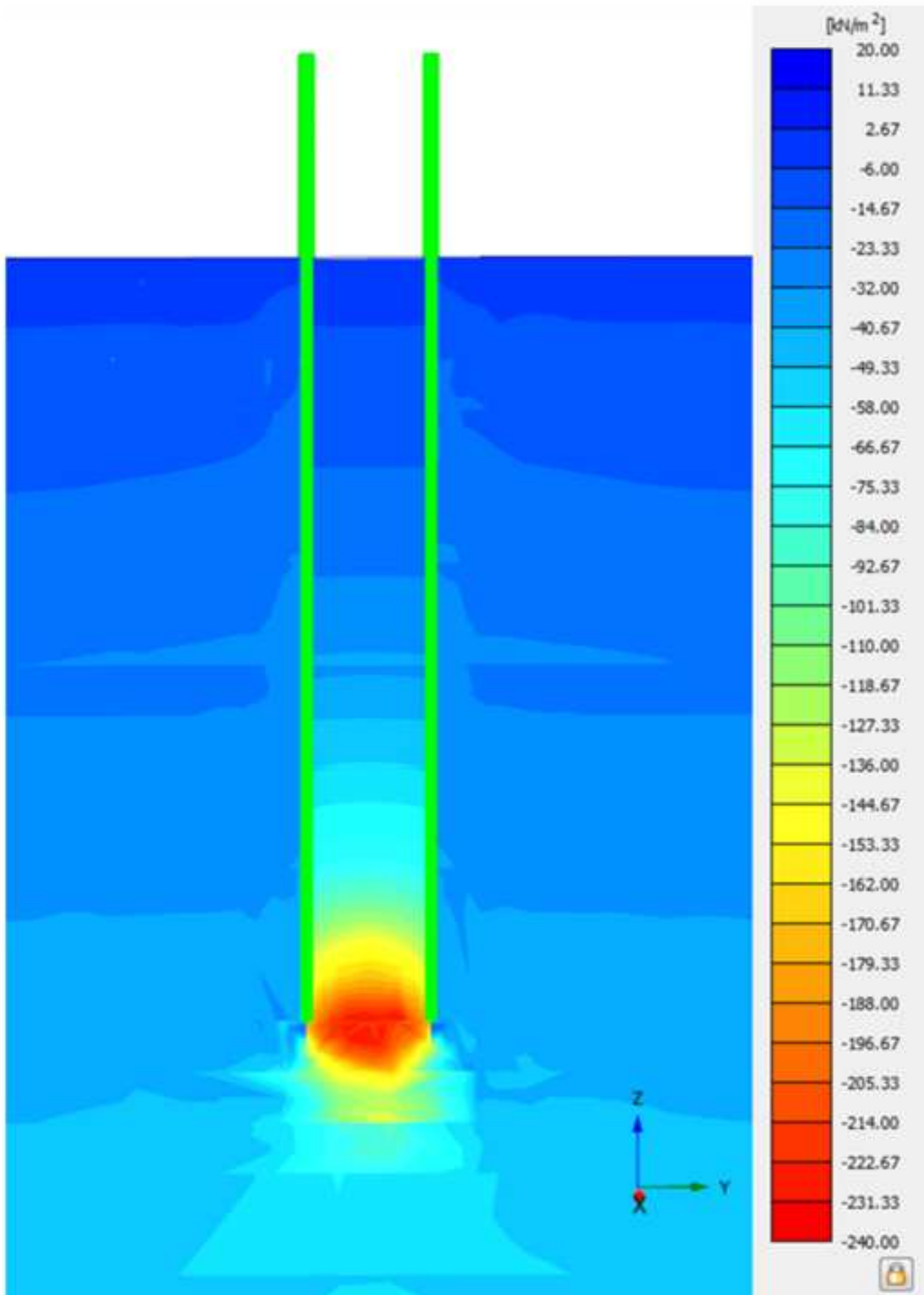


Figure
[Click here to download high resolution image](#)

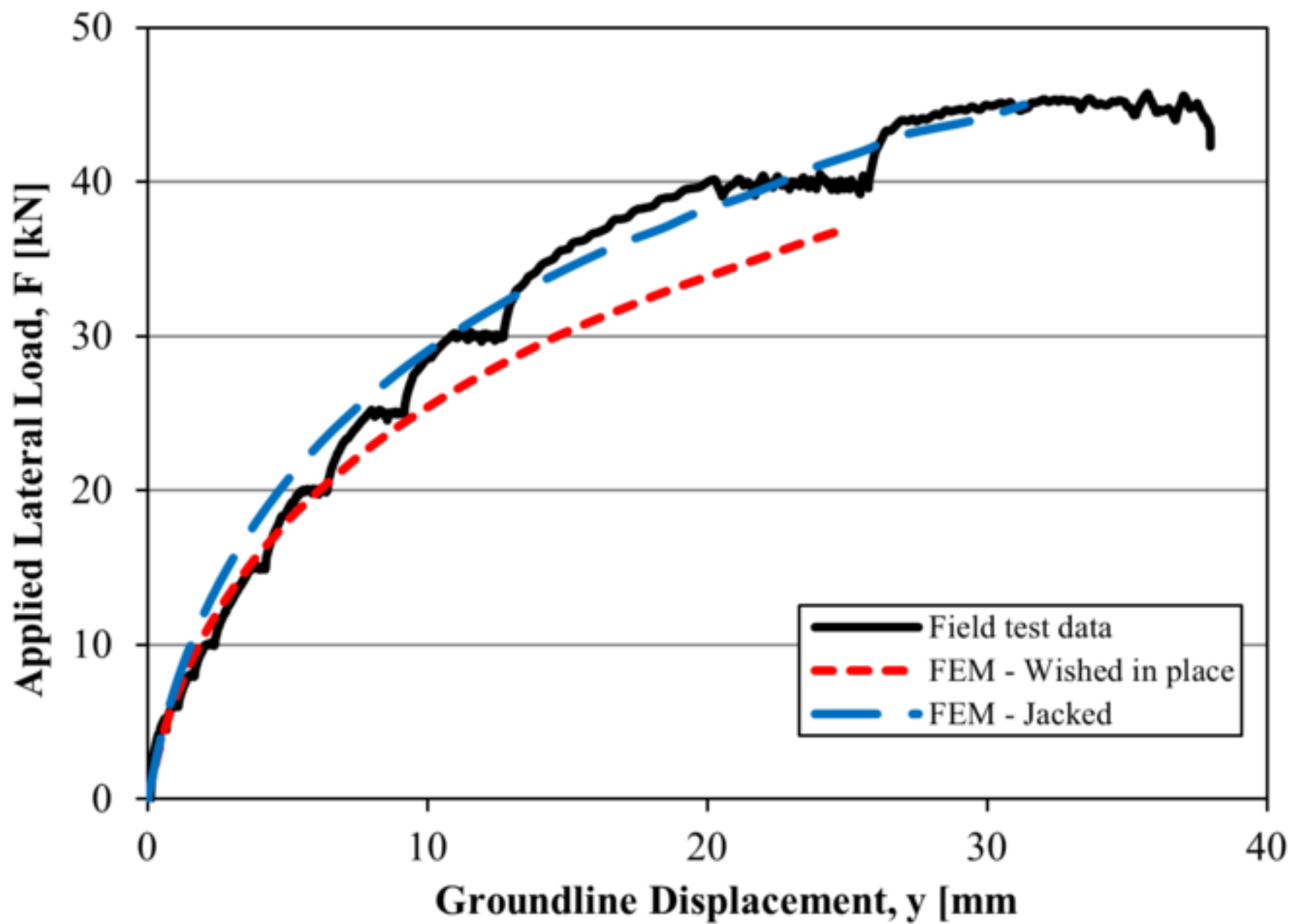


Figure
[Click here to download high resolution image](#)

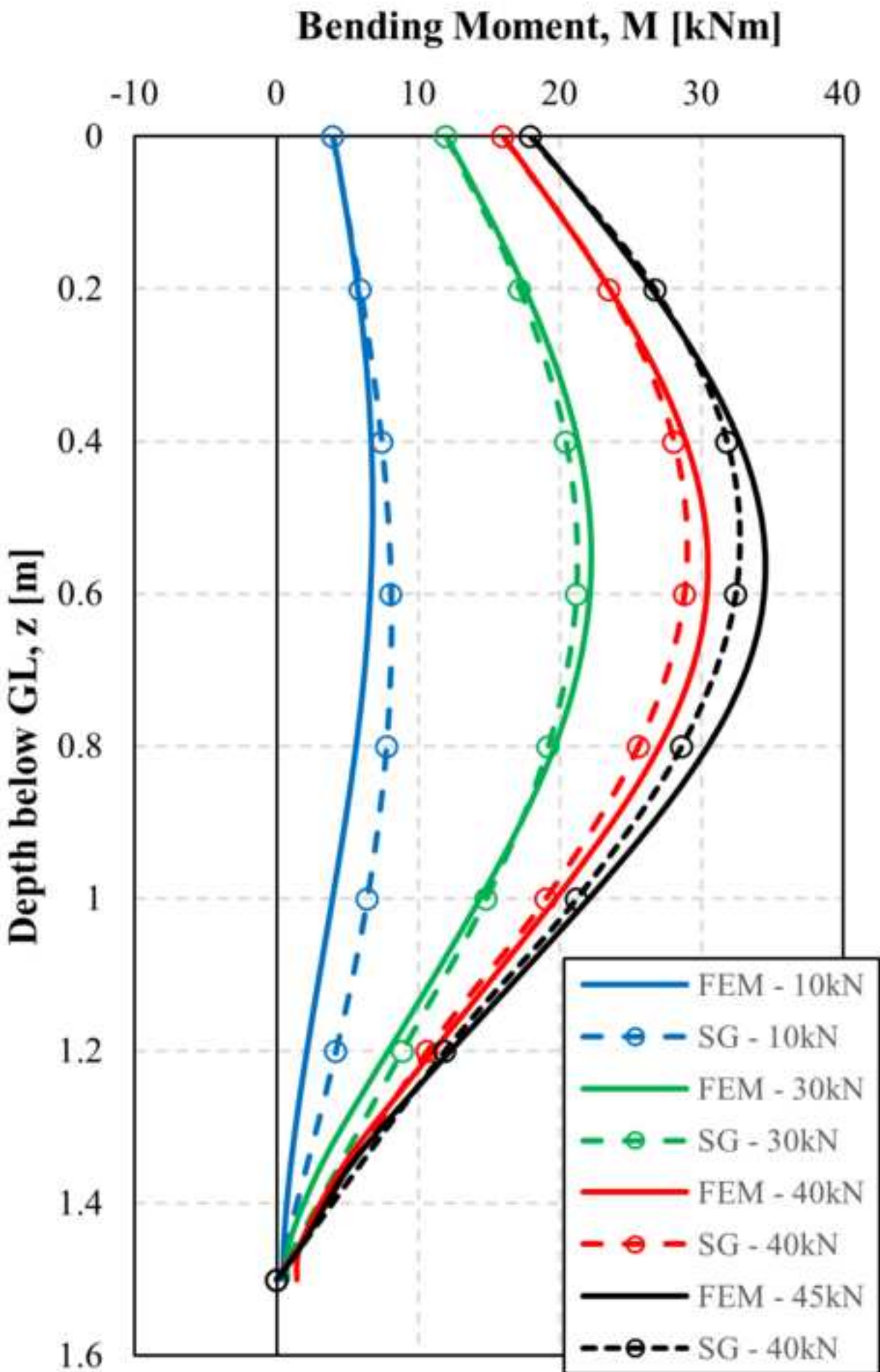


Figure
[Click here to download high resolution image](#)

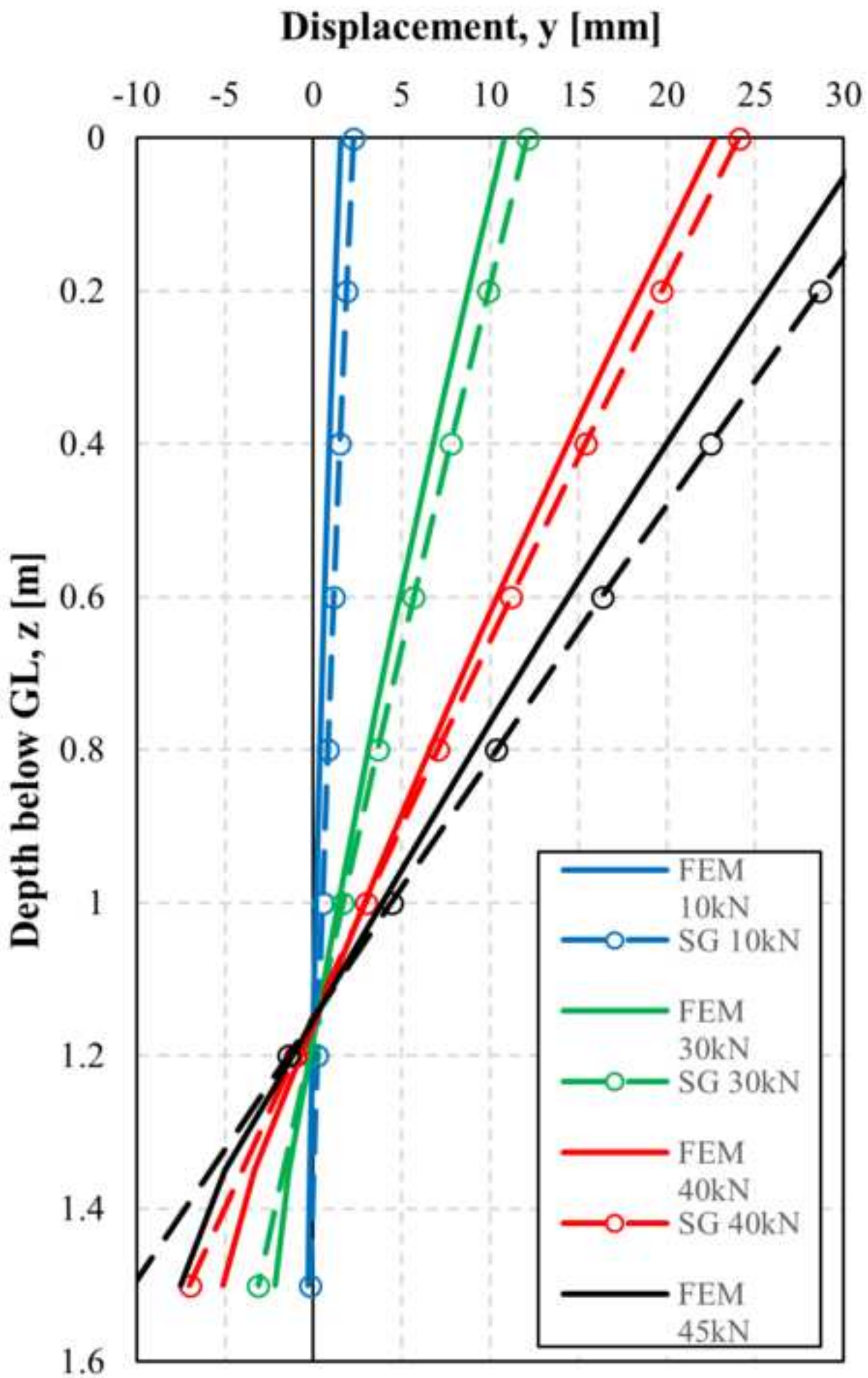


Figure
[Click here to download high resolution image](#)

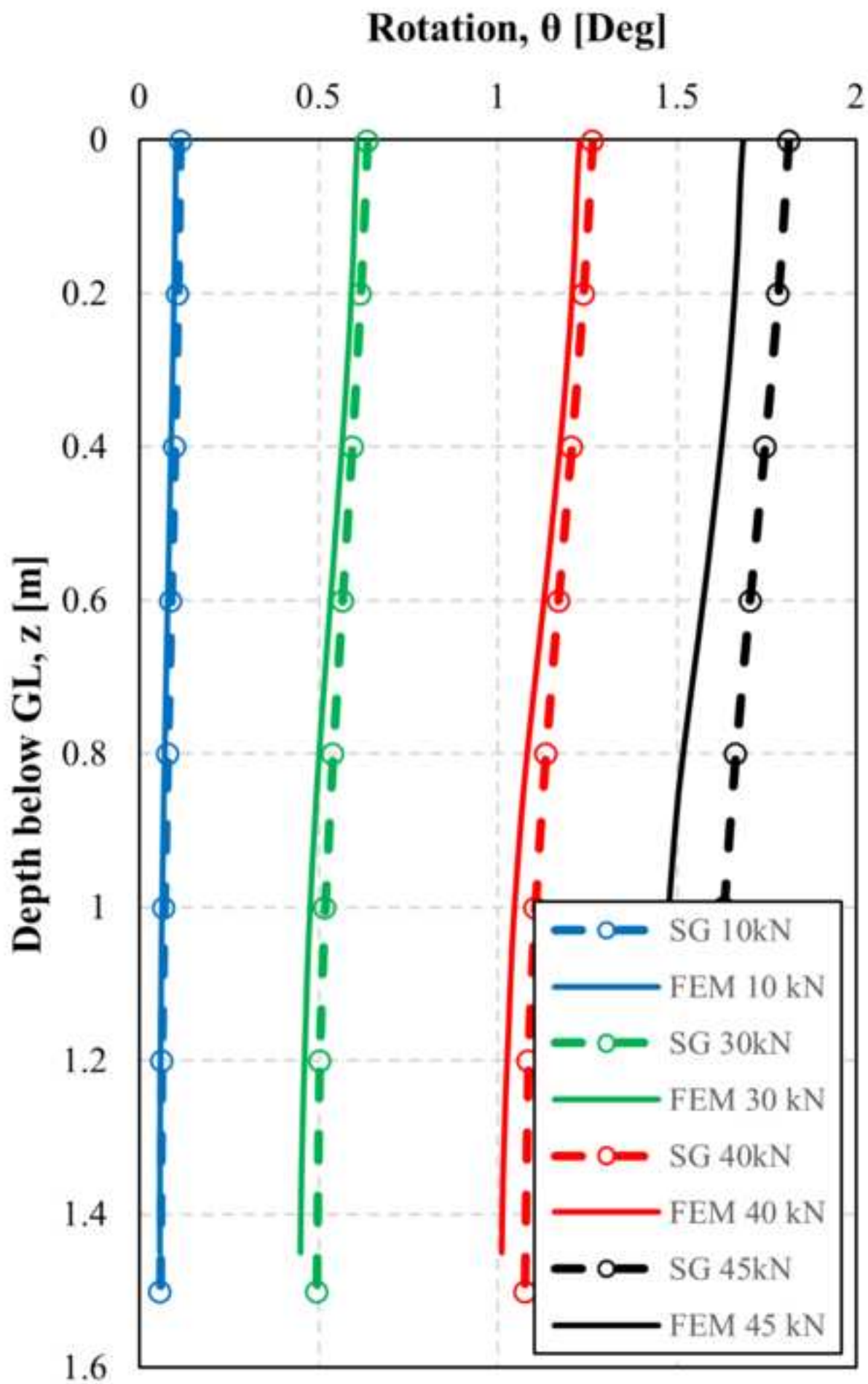
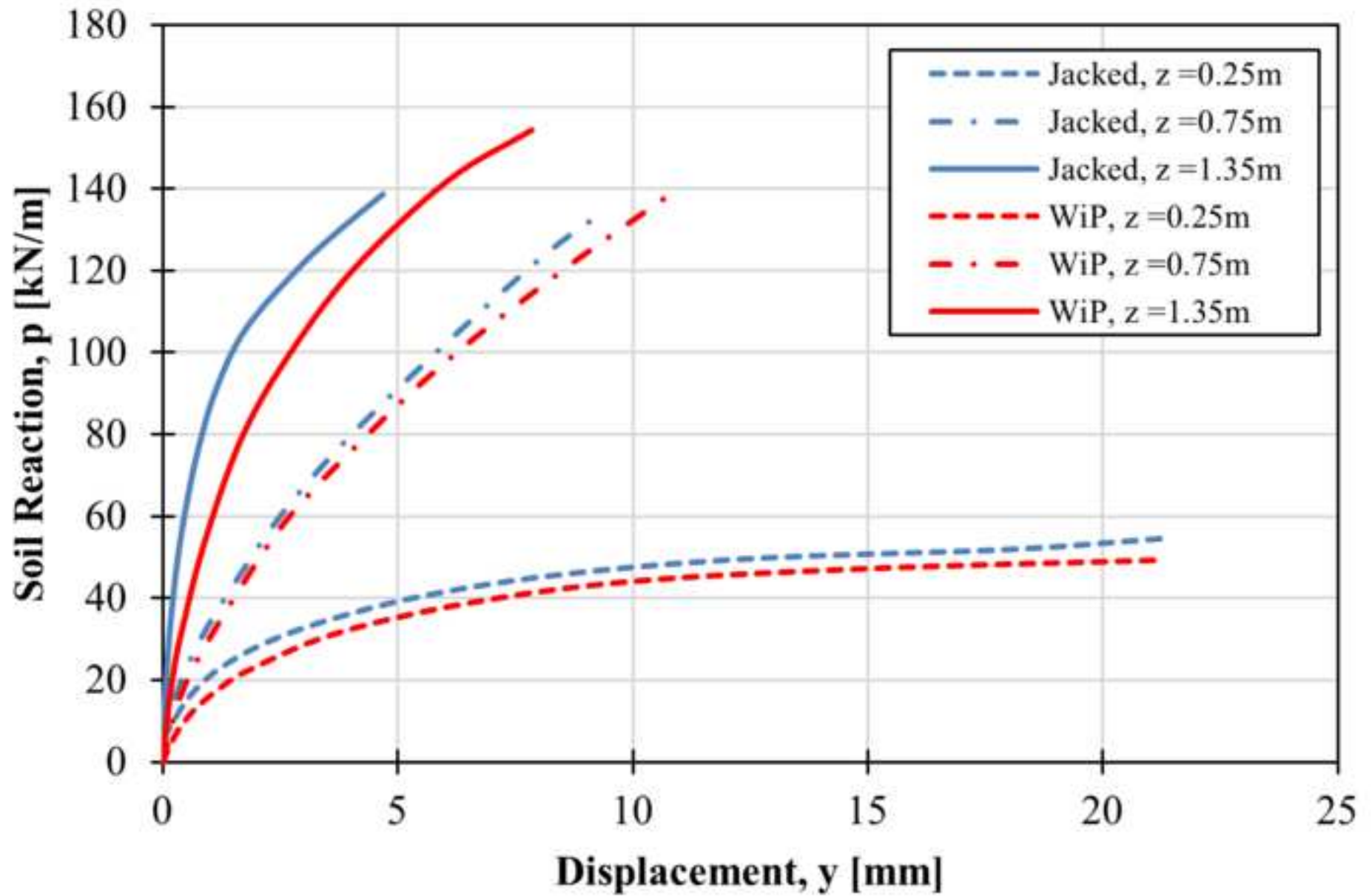


Figure
[Click here to download high resolution image](#)



Figure

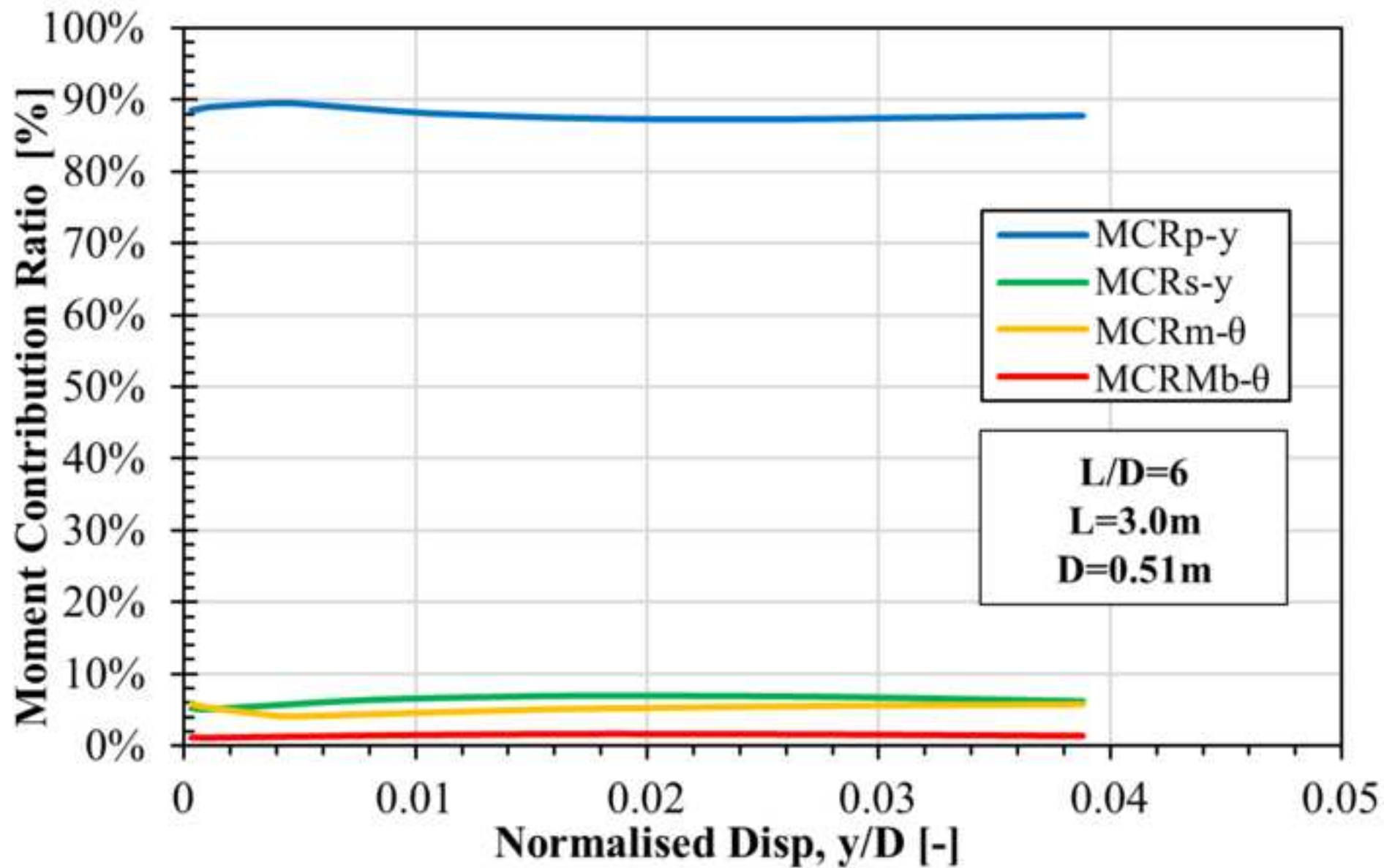
[Click here to download high resolution image](#)

Figure
[Click here to download high resolution image](#)

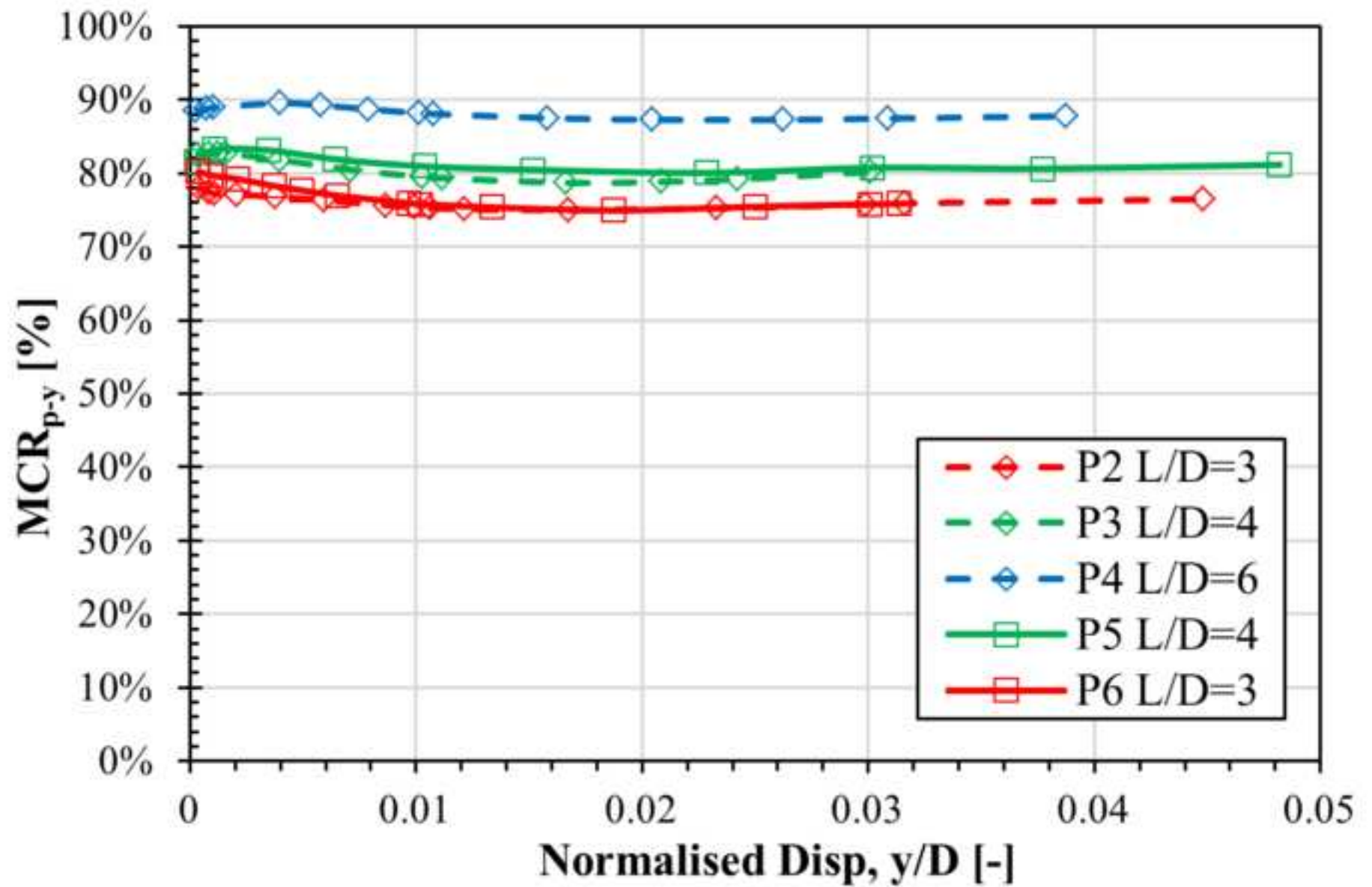


Figure
[Click here to download high resolution image](#)

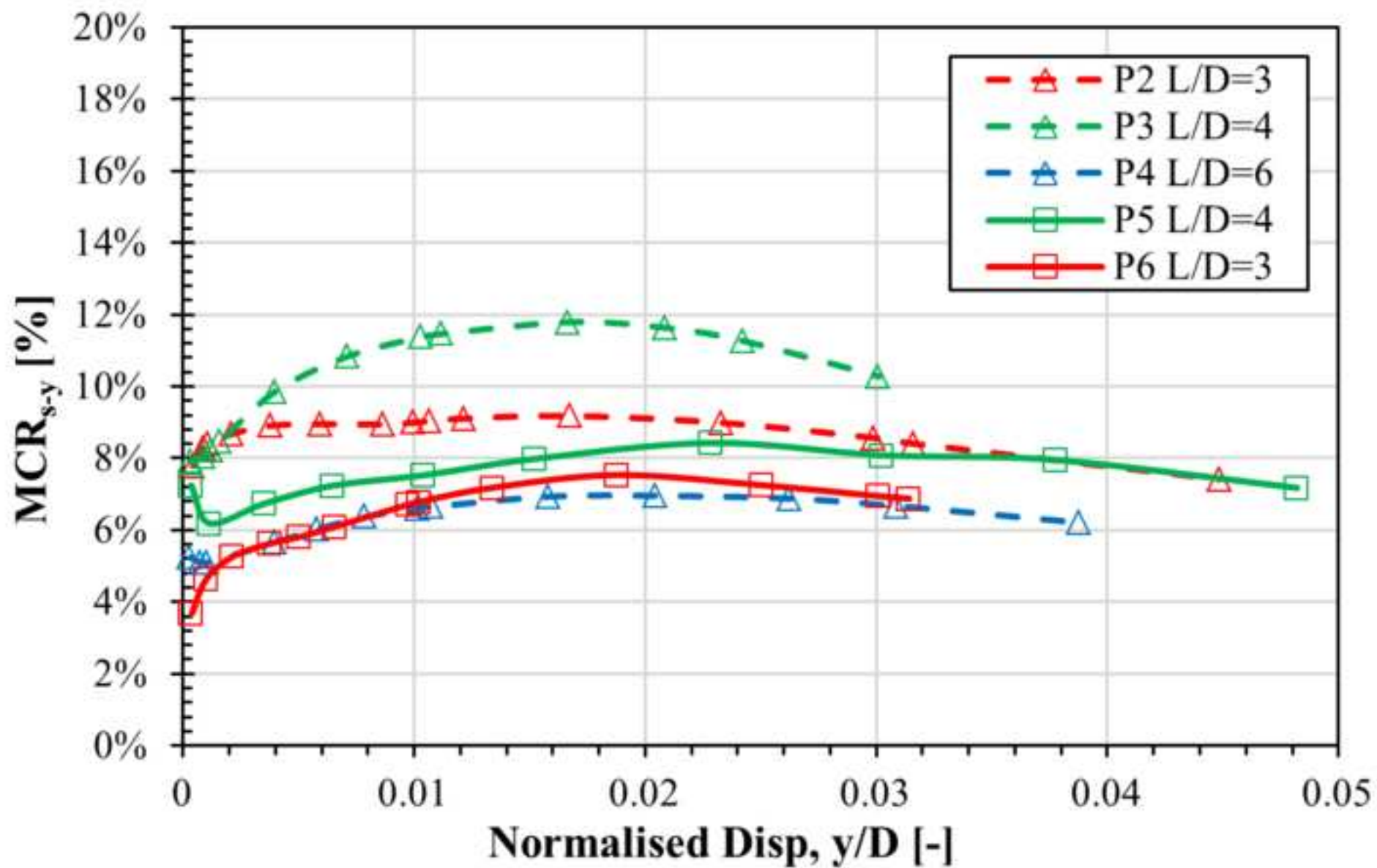


Figure
[Click here to download high resolution image](#)

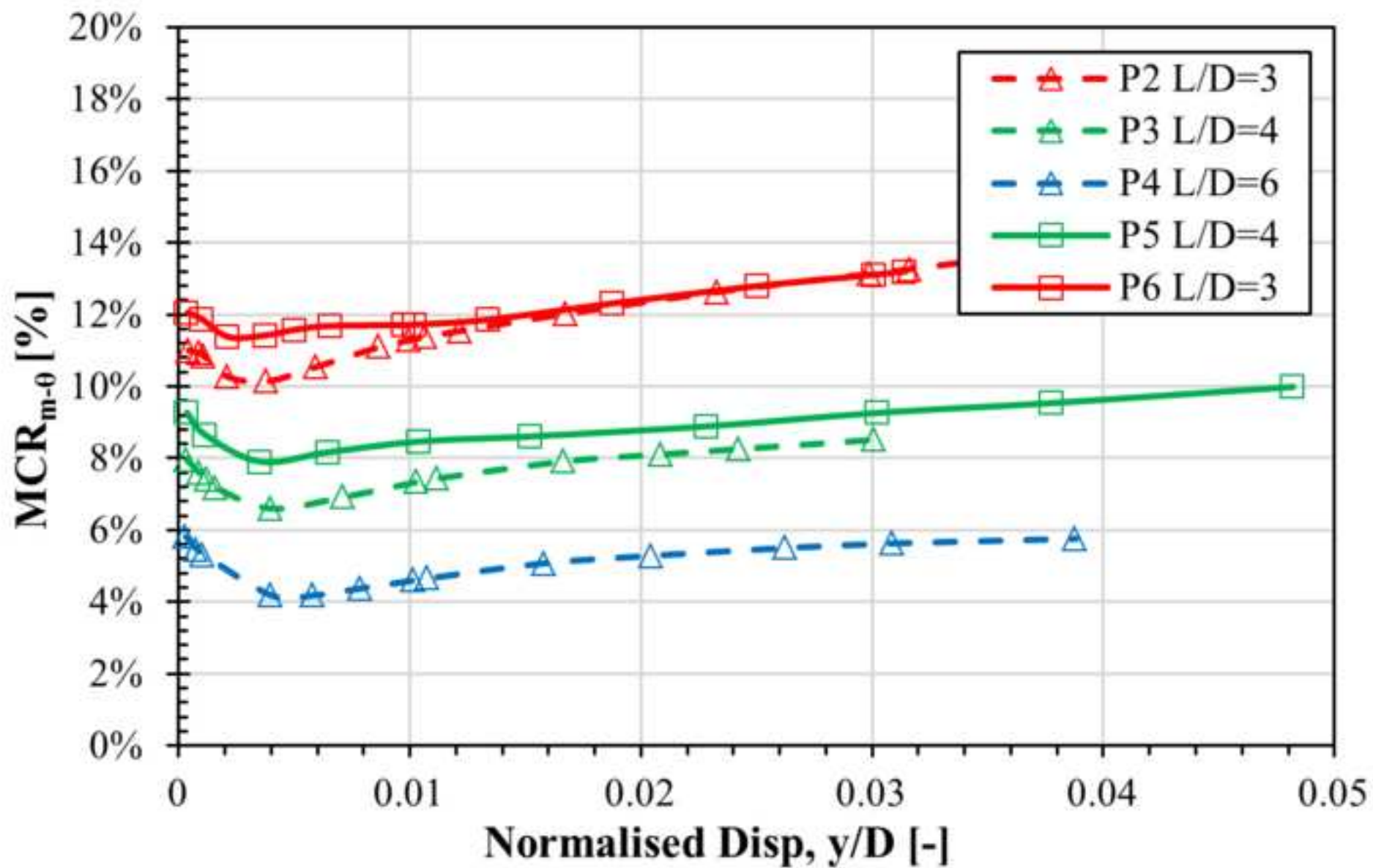


Figure
[Click here to download high resolution image](#)

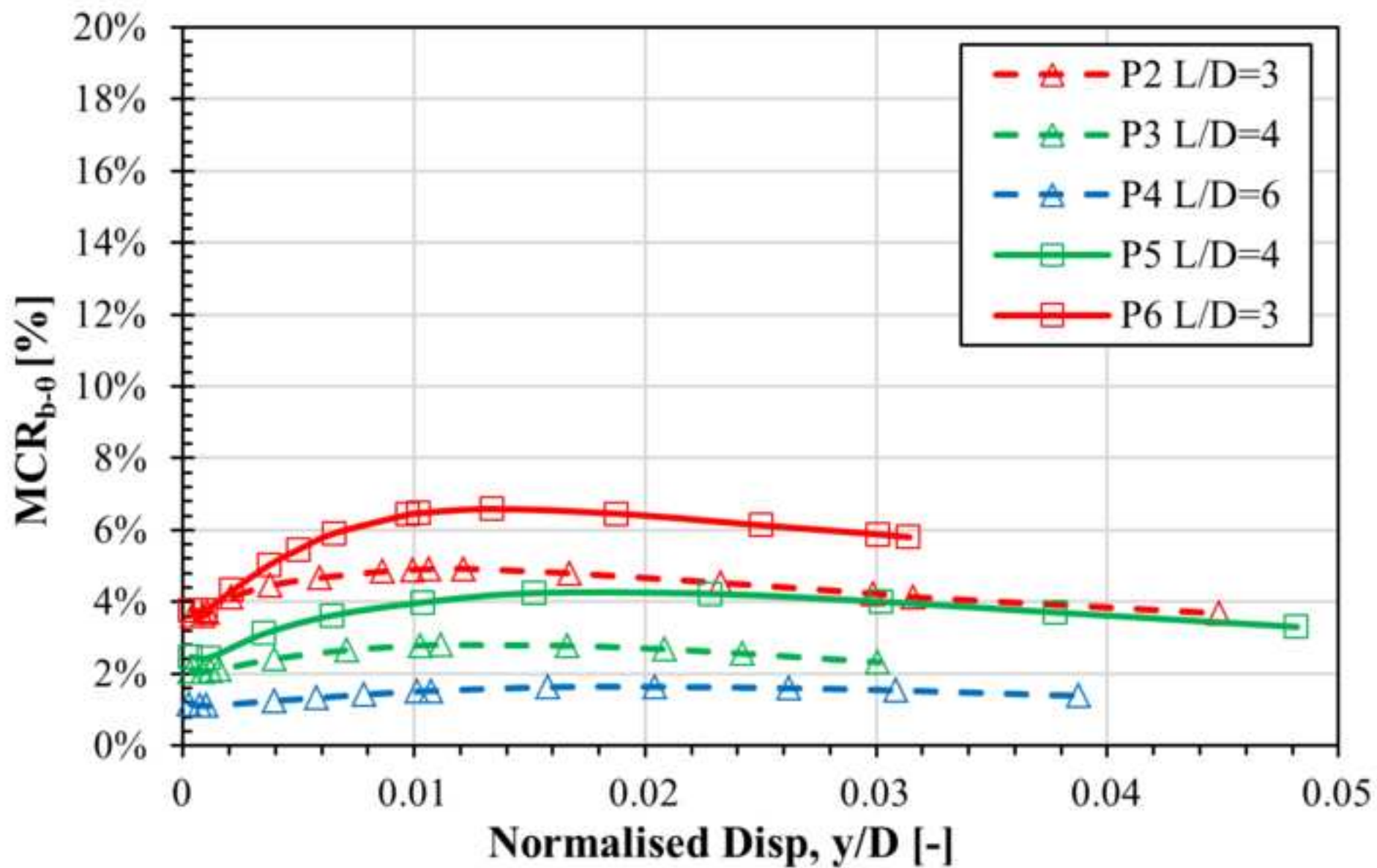


Table 1: Monopile Test Pile Dimensions

		Units	P1	P2	P3	P4
Embedded Length	L	mm	1500	1500	2250	3000
Diameter	D	mm	245	510	510	510
Wall Thickness	T	mm	8	10	10	10
L/D Ratio	-	-	6	3	4	6
Load eccentricity	h	mm	400	1000	1000	1000
Test location	-	-	Upper	Lower	Lower	Lower
FEM – Nodes	-	-	69367	139407	156147	148137
FEM – Elements	-	-	47218	95865	103795	100355

Table 2: Constant Soil Model Inputs

Parameter	Symbol	Units	Value
Effective soil weight	γ	kN/m ³	20
Effective Cohesion	c'	kN/m ²	0.1
Reference Stress	P_a	kN/m ²	100
Poissons Ratio	ν	-	0.2
Void ratio	e_{\max}	-	0.91
	e_{\min}	-	0.57
Interface Stiffness	R_{inter}	-	0.7